ACS APPLIED MATERIALS & INTERFACES

Biological and Medical Applications of Materials and Interfaces

Assembly of Building Blocks by Double-End-Anchored Polymers in the Dilute Regime Mediated by Hydrophobic Interactions at Controlled Distances

Emily Wonder, Kai K Ewert, Chenyu Liu, Victoria Marie Steffes, Jasmin Kwak, Vikar Qahar, Ramsey Majzoub, Zhening Zhang, Bridget Carragher, Clinton S. Potter, Youli Li, Weihong Qiao, and Cyrus R Safinya

ACS Appl. Mater. Interfaces, **Just Accepted Manuscript** • DOI: 10.1021/acsami.0c10972 • Publication Date (Web): 22 Sep 2020

Assembly of Building Blocks by Double-End-Anchored Polymers in the Dilute Regime Mediated by Hydrophobic Interactions at Controlled Distances

Emily A. Wonder,[1‡] Kai K. Ewert,[1‡] Chenyu Liu,[1,2] Victoria M. Steffes,[1] Jasmin Kwak,[1,a] Vikar Qahar,[1] Ramsey N. Majzoub,[1,b] Zhening Zhang[3,c], Bridget Carragher[3], Clinton S. Potter[3], Youli Li,[4] Weihong Qiao,[2] Cyrus R. Safinya[1]*

[1] Materials, Physics, and Molecular, Cellular, and Developmental Biology Department, University of California, Santa Barbara, California 93106, USA
[2] State Key Laboratory of Fine Chemicals, School of Chemical Engineering, Dalian University of Technology, Dalian 116024, P. R. China
[3] The National Resource for Automated Molecular Microscopy, Simons Electron Microscopy Center, New York Structural Biology Center, New York, NY 10027, USA
[4] Materials Research Laboratory, University of California, Santa Barbara, California 93106, USA

[a] Current address: Physics and Astronomy Department, University of California, Irvine, California 92697, USA
[b] Current address: Cryo-Electron Microscopy Center, Columbia University Irving Medical Center New York, 10032, USA
[c] Current address: Intellia Therapeutics, Cambridge, MA

‡ These authors contributed equally

* Corresponding author; email address: Safinya@mrl.ucsb.edu

Keywords:

PEG-lipid, liposomes, self-assembly, hydrophobic mediated tethering, tunable assembly, competing interactions, lipid membrane, lipid bilayer

Abstract

Hierarchical assembly of building blocks via competing, orthogonal interactions is a hallmark of many of nature's composite materials that do not require highly specific ligand-receptor interactions. To mimic this assembly mechanism requires the development of building blocks capable of tunable interactions. In the present work, we explored the interplay between repulsive (steric and electrostatic) and attractive hydrophobic forces. The designed building blocks allow hydrophobic forces to effectively act at controlled, large distances, to create and tune the assembly of membrane-based building blocks under dilute conditions and affect their interactions with cellular membranes via physical cross-bridges. Specifically, we employed double-end-anchored poly(ethylene glycol)s (DEA-PEGs)—hydrophilic PEG tethers with hydrophobic tails on both ends. Using differential-interference-contrast optical microscopy, synchrotron small angle X-ray scattering (SAXS), and cryogenic electron microscopy, we investigated the ability of DEA-PEGs to mediate assembly in the dilute regime on multiple length scales and on practical time scales. The PEG length, anchor hydrophobicity, and molar fraction of DEA-PEG molecules within a membrane strongly affect the assembly properties. Additional tuning of the intermembrane interactions can be achieved by adding repulsive interactions via PEG-lipids (steric) or cationic lipids to the DEA-PEG-mediated attractions. While the optical and electron microscope imaging methods provided qualitative evidence of the ability of DEA-PEGs to assemble liposomes, the SAXS measurements and quantitative line-shape analysis in dilute preparations demonstrated that the ensemble average of loosely organized liposomal assemblies maintains DEA-PEG concentration-dependent tethering on defined nanometer length scales. For cationic liposome–DNA nanoparticles (CL–DNA NPs), aggregation induced by DEA-PEGs decreased internalization of NPs by cells, but tuning the DEA-PEG-induced attractions by adding repulsive steric interactions via PEG-lipids limited aggregation and increased NP uptake. Furthermore, confocal microscopy imaging together with colocalization studies with Rab11 and LysoTracker as markers of intracellular pathways showed that modifying CL–DNA NPs with DEA-PEGs alters their interactions with the plasma and endosomal membranes.

Abbreviations

CL: Cationic liposome
Cryo-EM: cryogenic transmission electron microscopy
DEA-PEG: double-end-anchored poly (ethylene glycol)
DIC: differential-interference-contrast
DMEM: Dulbecco's modified Eagle's medium
DOPC: 1,2-dioleoyl-*sn*-glycero-3-phosphocholine
DOTAP: N-[1-(2,3-dioleoyloxy)propyl]-N,N,N-trimethylammonium chloride
NA: nucleic acid
NP: nanoparticle
PEG: poly (ethylene glycol)
SAXS: small-angle X-ray scattering
SEA-PEG: single-end-anchored poly (ethylene glycol)

Introduction

Many of nature's complex and sophisticated materials arise from the hierarchical assembly of simpler building blocks. In particular, a combination of competing, orthogonal interactions can give rise to remarkable and programmable complexity, without requiring the highly specific ligand-receptor interactions commonly associated with biological systems. To successfully mimic such hierarchical materials, it is necessary to develop building blocks that can produce the required, tunable interactions. While electrostatic interactions are tunable and long-range, they are also readily screened and have limited utility in many settings. In the present work, we explored introducing and tuning other nonspecific interactions in dilute solutions. In particular, we employed repulsive steric forces (mediated by poly(ethylene glycol)-lipid (PEG-lipid)) and attractive hydrophobic forces (acting at defined distances that are large for hydrophobic interactions; mediated by lipid–PEG–lipid macromolecules) to create and direct assembly of membrane-based building blocks. Further, we studied the interactions of the new assemblies with biological membranes inside and outside of the cell.

The specific systems that we investigated in regard to modifying intermembrane interactions were lipid carriers such as neutral and cationic liposomes and liposome–nucleic acid (NA) nanoparticles (NPs), which are relevant for delivery applications. Cationic liposomes (CLs; consisting of mixtures of cationic and neutral lipids) are a common synthetic carrier of hydrophobic small molecules as well as of nucleic acids (NAs) in therapeutic applications.[1-12] Gene therapeutics represent a paradigm shift in the treatment of many ailments, and recent discoveries, including RNAi gene silencing, mRNA vaccines, and CRISPR/Cas9 gene editing, have only increased the scope of this approach. However, delivery of the large, charged NAs that are readily susceptible to biochemical degradation poses a major challenge. Despite the fact that the capacity and safety profile of CL-based NA carriers are superior to those of viral vectors,[11,13-16] the first gene therapy (patisiran/ONPATTRO™) based on lipid vectors was approved for clinical use only as recently as 2018, after decades of worldwide effort.[17-19] Notably, patisiran addresses a therapeutic need that presents comparatively low challenges for delivery. To be applied more broadly, lipid vectors for therapeutic NAs require further research into their fundamental science aspects. This includes understanding their interactions with cellular membranes and the ability to modulate these interactions, which affect vector binding, uptake, trafficking, and endosomal escape.

The use of liposomes as drug or NA carriers *in vivo*, where the efficacy of viral vectors is typically superior, requires their stabilization against aggregation and opsonization. PEGylation (by incorporating PEG-lipids; Figure 1 (ii)) achieves this by sterically stabilizing liposomes[20-26] and NPs[27-31] and increases their circulation time *in vivo*. However, because the repulsive PEG corona counteracts any attractive interactions (such as van der Waals or electrostatic attraction), it also detrimentally affects desirable cell-nanoparticle interactions.[32-34]

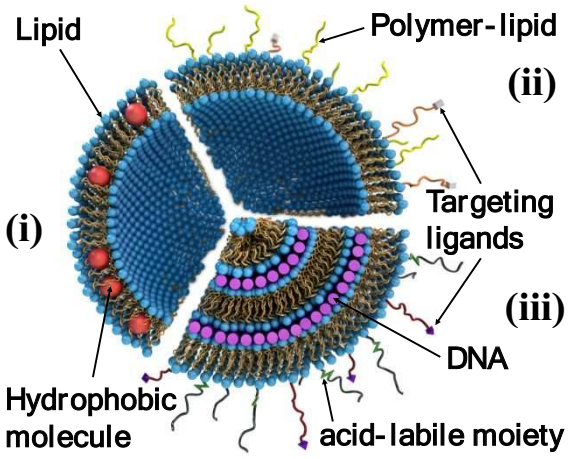

Figure 1. (i) A unilamellar liposome consisting of a self-assembly of amphiphilic lipid molecules. The liposome can carry hydrophobic molecules (red spheres) within its hydrophobic bilayer and hydrophilic molecules in its aqueous interior. **(ii)** A "stealth" liposome, where the lipid bilayer contains a small percentage of polymer-lipids to enable the surface-modified liposome to avoid immune cells. Such liposomes may also incorporate cell-targeting ligands (e.g., peptides or antibody fragments) attached to the distal end of the polymer-lipid. **(iii)** The lamellar L_{α}^{C} phase of CL–DNA complexes, consisting of an onion-like structure with DNA (purple rods) sandwiched between cationic membranes. In addition to cell-targeting ligands, surface functionalization may also include polymer-lipids with acid-labile, hydrolysable groups for shedding of the polymer in late endosomes after uptake of complexes by cells. Figure adapted from reference[4] by permission from The Royal Society of Chemistry (RSC) on behalf of the Centre National de la Recherche Scientifique (CNRS) and the RSC. Copyright 2014 RSC.

Important efficacy-limiting steps that rely on attractive cell–NP interactions are cell targeting/attachment (leading to uptake) as well as endosomal escape.[35,36] Prior work has shown that charge or surface functionalization by adding PEG-lipids with distally attached high-affinity peptides that specifically bind suitable cell surface receptors (Figure 1)[8,9,34,37-42] can provide the attractive interactions that enhance attachment to and uptake through endocytosis by cells. Similarly, charge or low-pH-cleavable PEG-lipids[33] (which unmask charge/reduce steric repulsion) can promote fusion with endosomal membranes. However, while (positive) charge is efficient in mediating interactions between NPs and cell membranes (which are anionic), the same nonspecific electrostatic attraction can compete with the specific binding of NPs to cells via high-affinity peptide-cell receptor interactions[39] and can result in rapid clearance of NPs from circulation. Thus, *in vivo* applications require low-charge NPs, i.e. NPs prepared close to but slightly above a CL/NA charge ratio of one. We reasoned that incorporating membrane-tethering elements into CL–NA nanoparticles could create attractions between the NP and endosomal membranes but do so without the detrimental effects of charge. A large body of work exists on associative polymers,

hydrophobically modified water-soluble polymers that can flocculate colloids and associate with liposomes.[43-45] These include PEG-based polymers, typically with a graft-copolymer structure with several hydrophobic groups per chain.[46,47] For our purposes, we envisioned that double-end-anchored PEGs (DEA-PEGs) – hydrophilic PEG with hydrophobic tails on both ends (Figure 2A), at least one of which being a double-tail unit that provides strong and stable membrane anchoring – could modulate intermembrane interactions via charge-independent, nonspecific interactions (physical cross-bridges). Conventional PEG-lipids have only one hydrophobic anchor (i.e., they may be considered single-end anchored PEGs (SEA-PEGs)) and therefore are purely repulsive. In contrast, the addition of a second hydrophobic anchor at the distal end of the PEG chain in DEA-PEGs introduces the potential for attractive interactions between apposing lipid membranes.[48-50] DEA-PEGs exhibit both looping and bridging conformations (Figure 2B) when incorporated into the membranes of bulk lamellar phases.[48,49] Small-angle X-ray scattering (SAXS) showed that the bridging (tethering) conformations limit the expansion (i.e., lock the interlamellar distance, d_W) of a multilamellar phase of positively charged membranes at high lipid concentrations, effectively inducing an attractive interaction between apposing membranes.[50] The resulting interlamellar distance is of order of the radius of gyration (R_G) of the PEG tether: $d_w \approx 1.6\, R_G = 1.6\, a\, n^{3/5}$, with a=3.6 Å the monomer length and n the degree of polymerization of the PEG tether.[50] Thus, it is possible to adjust the wall-to-wall spacing (controlling the range of interaction) between apposing membranes by varying the length of the PEG tether. Furthermore, the strength of the tethering increased with increasing concentration of DEA-PEG in the lipid membrane. Finally, varying the structure of the second anchor allowed us to modify the kinetics of phase formation (by modulating the stability of the intermediate state in Figure 2B) independent of the overall anchoring strength (which is modulated by the mol fraction of DEA-PEG in the membrane as well as the structure of the anchor).[50]

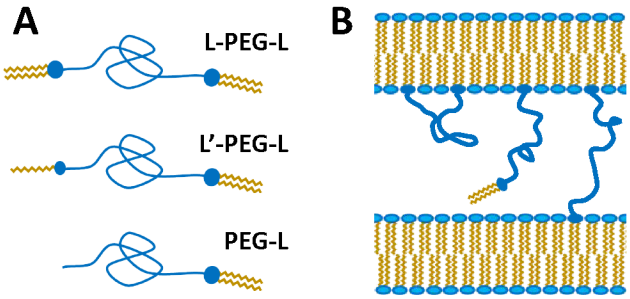

Figure 2. (A) symmetric (L-PEG-L) and asymmetric (L'-PEG-L) double-end-anchored (DEA)-PEGs and control PEG-lipid (PEG-L). **(B)** Schematic depiction of the conformations of DEA-PEG incorporated into apposing lipid membranes. DEA-PEGs may form looping (left; both hydrophobic tails in the same membrane) or bridging (right; hydrophobic tails in apposing membranes) conformations. These conformations can interchange through intermediate states with one anchor in the aqueous layer (center),

related to the barrier between conformations. The bridging conformation locks apposing membranes in close proximity in the presence of excess water.[48-50]

These studies provided proof-of-concept that incorporation of DEA-PEGs can provide attractive, nonspecific interactions of tunable strength and range. However, the experiments used bulk lamellar phases with high lipid concentrations (≥ 10 wt% in water) and required equilibration times on the scale of weeks.

In the present work, we sought to determine whether the attractive interaction mediated by DEA-PEGs is applicable in the context of liposomes and lipid-based NPs (i.e., the dilute regime of lower lipid concentrations) and their applications (i.e., shorter time scales), such as drug and gene delivery. Thus, we characterized the ability of DEA-PEGs to mediate assembly of liposome-based building blocks in dilute systems by tuning hydrophobic, steric, and electrostatic interactions. To do so, we varied the PEG length, anchor hydrophobicity, and molar fraction of DEA-PEGs within a membrane. In addition, we tuned the steric and electrostatic interactions between the membranes by the incorporation of charged lipids and PEG-lipids. We used differential-interference-contrast-microscopy (DIC), synchrotron SAXS, and cryogenic transmission electron microscopy (cryoEM) to characterize the lipid assemblies, demonstrating tunable DEA-PEG-mediated hierarchical assembly in both loosely organized dilute liposomal systems and highly organized, liquid crystalline lipid–NA systems. In addition, confocal microscopy with fluorescence colocalization using Rab GTPases and LysoTracker as markers of endosomal organelles[51] revealed the DEA-PEGs mediate attractive interactions between CL–DNA NPs and showed that the colocalization (i.e., endosomal trafficking) pattern of NPs is modified by the presence of DEA-PEGs.

Materials and Methods

Materials

The lipids DOPC (1,2-dioleoyl-*sn*-glycero-3-phosphocholine) and DOTAP (N-[1-(2,3-dioleoyloxy)propyl]-N,N,N-trimethylammonium chloride) were purchased from Avanti Polar Lipids as a solution in chloroform. Paclitaxel was purchased from Acros. Pentavalent MVL5,[52] SEA-PEGs,[50] and DEA-PEGs[50] were synthesized as previously described. The structures of all the lipids used in this work are shown in Figure S1 in the Supporting Information. High-resistivity (18.2 MΩcm) water was obtained from a Milli-Q Plus unit (Millipore).

The pGFP plasmid used to form the CL–DNA complexes was purchased from Promega, and the Rab11–GFP plasmid was purchased from Addgene. LysoTracker Red was purchased from Life Technologies. Poly-L-lysine (Sigma-Aldrich) was used to coat glass slides prior to seeding cells for microscopy studies.

Liposome and DNA Preparation

Stock solutions of MVL5 and PEG-lipids were prepared by dissolving the lipid in a chloroform:methanol mixture (3:1, v/v). Paclitaxel was dissolved in chloroform to prepare a stock solution at 10.0 mM. To prepare liposomes of the desired compositions, stock solutions were combined at the desired molar ratio, and the organic solvent was evaporated by a stream of nitrogen followed by overnight (12–16 h) incubation in a vacuum. The appropriate amount of high resistivity water to achieve the desired lipid concentration was added to the dried lipid film, and the hydrated films were incubated overnight at 37 °C to form liposomes. The liposome suspension was then sonicated, either using a tip sonicator for 5–20 min or a bath sonicator for 30–60 min. Sonication times varied and were determined by the length of sonication necessary for opaque suspensions to become transparent (or translucent for highly concentrated suspensions). This sonication method is the same as in previous investigations of drug and NA delivery with liposomes; sonication can be performed on small (≈100 μL) sample volumes with minimal loss of material and does not use filters that may be blocked by aggregates. Liposome suspensions for incubation with cells were prepared at 0.95 to 1.0 mM, while suspensions for nanostructure characterization (i.e., differential interference contrast microscopy, small angle X-ray scattering, cryogenic electron microscopy) were prepared at 19 to 20 mM.

All plasmids were propagated in *Escherichia coli* and purified using Qiagen Giga or Mega Prep kits. For microscopy studies, the pGFP plasmid was labeled with Cy5 following plasmid purification using the Mirus Bio Label IT nucleic acid labeling kit according to the manufacturer's protocol with one modification: the incubation time at 37 °C was increased from 1 to 2 h to improve labeling efficiency.

Differential Interference Contrast Microscopy

A total of 400 μL of liposome solution (≈19 mM) was prepared for both differential interference microscopy and small angle x-ray scattering. The solution was mixed with a pipette, and a total of 3 μL was placed between a glass microscopy slide and a coverslip which was sealed with vacuum grease. At the time of imaging, the solutions had been tip-sonicated twice. The solution was imaged with a Nikon Diaphot 300 equipped with 10× DIC Objective and Sensicam QE CCD camera (PCO).

Small Angle X-ray Scattering

Liposomes were prepared at a concentration of ≈19 mM and tip-sonicated once. Samples were mixed with a pipette, loaded into 1.5 mm quartz capillaries (Hilgenberg). The capillaries were centrifuged at 10 000 *g* for 30 min to increase liposome density and then sealed with epoxy resin. Sample scattering was measured at several heights of the capillary to investigate the macroscopic separation and concentration of different phases resulting from centrifugation.

SAXS measurements were carried out at the Stanford Synchrotron Radiation Lightsource, beamline 4–2 at 9 keV (λ=1.3776 Å) with a Si(111) monochromator. Scattering data were taken with a 2D detector (Pilatus 3 X 1M, Dectris) with a sample to detector distance of ≈3.5 m (calibrated with silver behenate). The X-ray beam size at the sample was 150 μm in the vertical and 200 μm in the horizontal direction. Data reduction and analysis were performed using the NIKA and IRENA software packages developed at Argonne National Laboratory.[53,54] Line-shape analysis of the SAXS data was performed using custom-written code implemented in the Python programming environment. The scattering background was determined by a linear line drawn between the minima of the form factor at ≈0.04 $Å^{-1}$ and ≈0.2 $Å^{-1}$. The model was fit to the background-subtracted data.

Cryogenic Electron Microscopy

Liposome solutions for electron microscopy were prepared at a concentration of 20 mM. The cationic liposome sample was bath-sonicated. The CL–DNA sample was composed of tip-sonicated liposomes mixed with DNA. Samples were vitrified using a manual plunger on carbon lacey substrates (300 mesh copper grids) prepared in house.[55] Grids were plasma cleaned using O_2 and H_2 for 30 s using a Solarus plasma cleaner (Gatan) immediately prior to sample preparation. A total of 3 μL of sample was applied to the grid and manually blotted from the back with filter paper for 5 s, followed immediately by plunging into liquid ethane. Images were acquired using Leginon[56] on a Tecnai T12 electron microscope operated at 120 KeV and equipped with a 4K TVIPS CMOS camera. Images were collected at nominal magnification of 68 k ×, corresponding to a pixel size of 2.46 Å/pixel.

Cell culture and confocal imaging of fixed cells

PC-3 cells (ATCC number: CRL-1435; human prostate cancer) were cultured in DMEM (Invitrogen) supplemented with 10% (v/v) fetal bovine serum (Gibco) and 1% (v/v) penicillin/streptomycin (Invitrogen). Cells were passaged every 72 h to maintain subconfluency and kept in an incubator at 37 °C in a humidified atmosphere containing 5% CO_2.

Preparation of cells for confocal imaging with labeled Rab11 and late endosome/lysosome pathways has previously been described.[38] Prior to seeding cells, 22×22 mm No. 1.5 glass coverslips were coated with poly-L-lysine. PC-3 cells were seeded on the coated coverslips in 6-well plates (~140,000 cells/well) such that the confluency was 60–80% at 24 h after seeding. At 24 h after seeding, complexes were formed by mixing 10 μL of Lipofectamine 2000 (Life Technologies) with 4 μg Rab11–GFP plasmid. Lipofectamine 2000/pRab11–GFP complexes were added to cells in serum-free medium and removed 6 h later, according to the manufacturer's protocol. After removal of the Lipofectamine complexes, cells were washed with PBS and incubated in serum-containing medium overnight. The next day, cells were washed

and serum-containing medium was added again. At 48 h after transfection, fluorescently labeled NPs were prepared by mixing 2.4 μg of unlabeled pGFP with 0.6 μg of Cy5-labeled pGFP to produce a solution of 3 μg DNA in 250 μL of serum-free medium. The appropriate amount of liposome solution (0.95 to 1 mM; volume based on charge ratio and stock lipid concentration) was diluted to 250 μL in serum-free DMEM. Liposome and DNA solutions were mixed together and incubated at room temperature for 20–30 min to form NPs. The six-well plates containing seeded coverslips were removed from the incubator and washed once with PBS. A total of 2 mL of serum-free medium and 500 μL of NP suspension were added to each well, and cells were placed in the incubator. After 4.5 h of incubation, cells were removed and rinsed once with PBS. Following PBS washing, 2 mL of serum-free medium containing 50 ng/mL of LysoTracker Red (Life Technologies) was added to each well. Cells were incubated at 37 °C for 30 min in the presence of Lysotracker Red to allow for labeling of acidic organelles. After acidic organelle labeling, cells were washed twice with PBS and fixed using a PBS solution containing 3.7% (v/v) formaldehyde. Cells were incubated in the presence of formaldehyde for 10 min at room temperature with occasional agitation. After fixation, cells were washed with PBS three times and mounted onto slides using Antifade mounting medium (Life Technologies). The antifade medium was cured overnight and coverslips were sealed to the glass slides using a fast-curing epoxy resin.

Cells were imaged within 5 days of fixation using an Olympus DSU microscope equipped with a 100× UPlanSApo objective, a Hamamatsu ImagEM CCD camera, and Metamorph software. Representative cells were chosen and imaged at z-steps of 1 μm. Prior to colocalization analysis, images were processed as follows. First, the z-stacks were deconvolved using the ImageJ plug-in Iterative Deconvolve 3D. Processing after deconvolution consisted of a background subtraction with a 10-pixel rolling ball radius as well as a smooth filter for improved image clarity. Colocalization analysis was performed using custom-written Matlab routines and is described below.

Colocalization Analysis

Object-based colocalization analysis[33,34,38,51,57] was performed on 20–30 cells per NP composition. A rough outline of each cell was generated from an image produced by subtracting the NP channel from a saturated image of the Rab channel. This subtraction step allows automatic location of the cell boundary while excluding extracellular NPs, which form a thick fluorescent coat on the outside of the plasma membrane.[58] The Matlab routine prompts the user to mask neighboring cells in close proximity to the cell of interest and to set the bottom and top slice of each cell. For our analysis, we selected z-stack regions that were 2–3 μm thick. For each slice, NPs were located using a Matlab version of the algorithm first reported by Crocker and Grier.[59] Next, particles were given z-coordinates based on their brightness in

each stack (some NPs are visible at more than one height). Following the generation of a list of acidic organelle, recycling endosome, and NP coordinates, NPs were counted as colocalized with a marker (e.g., Lysotracker) if they were within three pixels of that marker and at least five pixels away from the other marker (e.g., Rab11–GFP). In all samples, a small fraction of NPs (<12%) colocalize with both markers due to the inability to resolve NPs in organelles that are too closely spaced in the x-y-plane of the microscope. NPs were not designated any colocalization ("Neither") if they were at least five pixels away from both markers. The colocalization statistics were calculated by dividing the total number of colocalized NPs by the total number of intracellular NPs. This method for averaging, as opposed to single-cell statistical averaging, is analogous to how transfection efficiency is measured with luciferase. (Luciferase expression measurements lack single-cell statistic due to cell lysis during harvesting.) The error for colocalization fractions is estimated at ±2%, as found for one sample that was imaged and analyzed twice.

Results and Discussion

DEA-PEGs

We have previously prepared symmetric and asymmetric DEA-PEGs (Figure 2) from PEG of molecular weight 2000 and 4600 g/mol (n=45 and 104), together with the corresponding SEA-PEGs.[50] As shown in Figure S1 in the Supporting Information, the symmetric DEA-PEGs (L-P2000-L and L-P4600-L) incorporate two dioleyloxybenzoic acid (DOB; double chain C18:1) tails, while the asymmetric DEA-PEGs (L'-P2000-L and L'-P4600-L) incorporate a DOB tail (L) and an oleic acid tail (L'; single chain C18:1). Single- and double-chain tails vary greatly in their water solubility (consider, e.g., the critical micelle concentration of lipids and surfactants, which differs by several orders of magnitude), which affects the stability of the intermediate conformation (Figure 2B). Also of note, none of the SEA- and DEA–PEGs bear a charge (unlike the commercially available DOPE-PEGs, which are anionic).

Optical Microscopy

For an initial assessment of whether the DEA-PEGs could exert attractive forces on liposomal building blocks, leading to aggregates by directed assembly, we turned to optical microscopy. Figure 3 displays DIC micrographs of samples prepared from lipid mixtures containing an increasing amount of the DEA-PEG L-P4600-L in the membrane. All liposomes were cationic, containing 10 mol% of the multivalent cationic lipid MVL5[52] in their membranes (molar composition: MVL5/DOPC/L-P4600-L=10/90-x/x). (Note that addition of PEG-lipid reduces the zeta-potential of cationic liposomes (but not to zero at low-salt conditions) but also adds steric repulsion.[60]) Control liposomes (x=0, without PEG-lipid or DEA-

PEG) form mostly small and very small unilamellar liposomes upon sonication that remain readily dispersed because of their charge. While these liposomes are readily observed in cryo-EM (see Figure S2 in the Supporting Information), they are not detected in our optical imaging experiments because of their submicrometer size. However, at 1 mol% of DEA-PEG in the lipid mixture, (comparatively small) aggregates are observed (Figure 3, x=1), together with a number of spherical objects that may be large liposomes. As the amount of DEA-PEG in the membrane increases, these spherical objects disappear and the size of the aggregates increases. A similar trend was observed for the other DEA-PEGs (see also Figure 4 (left, 10% MVL5)), with L'-P2000-L showing the least concentration dependence.

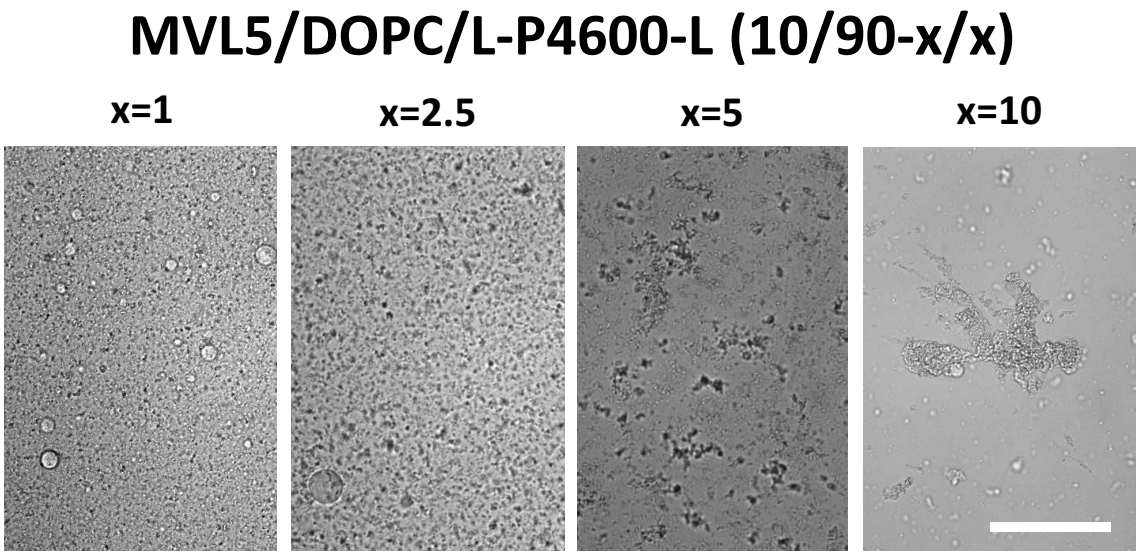

Figure 3. Differential-interference-contrast micrographs of suspensions of cationic liposomes containing varied amounts of the DEA-PEGs L-PEG4600-L (liposome composition: MVL5/DOPC/L-P4600-L (10/90-x/x)). As the amount of DEA-PEG in the membrane increases (left to right), aggregates of increasing size are observed. Plain control liposomes and those with PEG lipids form small liposomes (< 1 μm; see also Figure S2 in the Supporting Information) and are not detected with this imaging technique. Scale bar: 200 μm.

Having established that the DEA-PEGs introduce an attractive intermembrane interaction in a concentration-dependent manner, we sought to identify competing repulsive interactions that can be used to tune the interactions between DEA-PEG-containing liposomes. First, we investigated the effect of membrane charge density by increasing the amount of cationic lipid in the membrane. The membrane charge density of 50% DOTAP/50% DOPC membranes is higher than that of 10% MVL5/90% DOPC membranes.[61] (The membrane charge density of 50% MVL5/50% DOPC membranes is slightly higher than that of membranes containing 100% DOTAP.) As evident in Figure 4, increasing the membrane

charge density strongly reduced the formation of aggregates. While some smaller aggregates are still visible at 50% DOTAP, none are observed at 50% MVL5. This means that at this high membrane charge density, the electrostatic repulsion (in plain water; this repulsive force is readily and strongly modulated by the ionic strength in solution) was able to completely overcome the attractive forces exerted by the DEA-PEG.

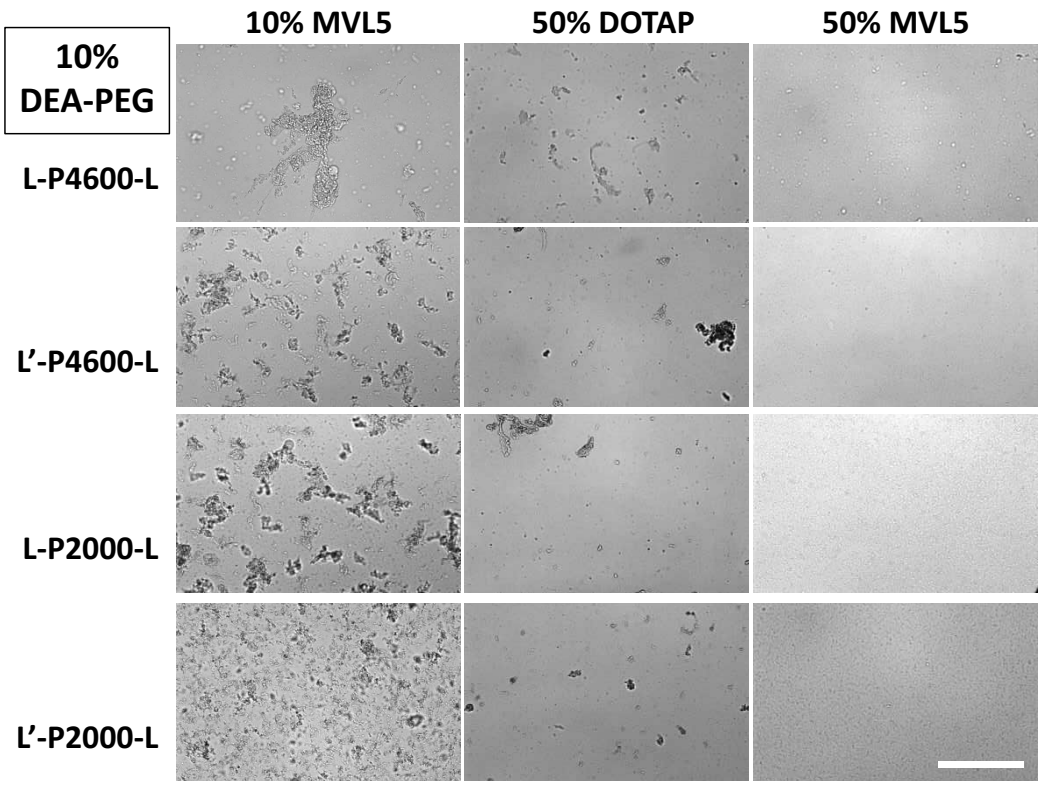

Figure 4. Differential-interference-contrast micrographs of suspensions of cationic liposomes of varied charge density, containing 10 mol% of DEA-PEG in the membrane. The liposome compositions were: cationic lipid/DOPC/DEA-PEG=x/90-x/10 (x=10 and 50 for MVL5 and x=50 for DOTAP. As the charge density of the membranes of the DEA-PEG-containing liposomes increases (left to right), the aggregates become fewer and smaller. (Small liposomes (< 1 μm) are not detected with this imaging technique, leaving a flat, gray background.) Scale bar: 200 μm.

We returned to membranes of low charge density (10% MVL5) to attempt to tune the DEA-PEG-induced interactions by introducing steric repulsion. To this end, we added a PEG-lipid (L-P2000; i.e., an SEA-PEG) of identical PEG chain length to membranes containing 5 mol% of the L'-P2000-L that very effectively tethers membranes[50] (see also the sections below). As evident from Figure 5, increasing concentrations of added SEA-PEG led to an increasing dispersion of aggregates. While strong

aggregation is still observed with 1 mol% SEA-SEA, the aggregates are smaller at 2.5 mol% and even smaller at 5 mol%.

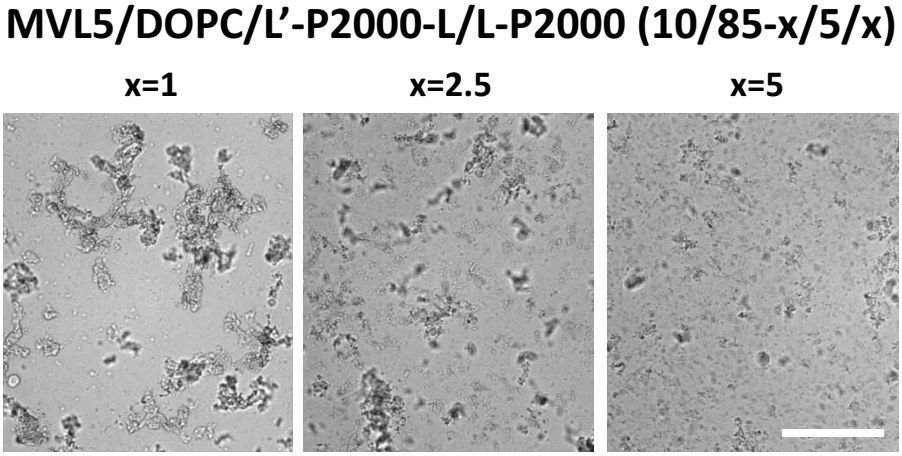

Figure 5. Differential-interference-contrast micrographs of suspensions of cationic liposomes containing varied amounts (1, 2.5 and 5 mol%) of PEG-lipid (SEA-PEG; L-P2000) in addition to 5 mol% of DEA-PEG (L'-P2000-L) in the membrane. The liposome compositions were: MVL5/DOPC/L'-P2000-L/L-P2000=10/85-x/x (x=1, 2.5, and 5). As the amount of (repulsive) SEA-PEG in the membranes of the DEA-PEG-containing liposomes increases (left to right), the aggregates become smaller. Scale bar: 200 μm.

Small Angle X-ray Scattering

To investigate DEA-PEG-induced aggregation at length-scales from ≈2 to 3 nanometers to as large as 250 nm, we turned to small-angle X-ray scattering (SAXS) of neutral and cationic liposomes (no and 10 mol% DOTAP, respectively) with varying DEA-PEG content. The synchrotron SAXS data was collected between q=0.0025 Å^{-1} and q=0.2 Å^{-1}, which probes length scales (of the order of ≈2π/q) between ≈2,500 Å and ≈30 Å. DIC imaging covers the length-scale range from about 0.25 μm (i.e., limited by wavelength/2) to >100 of μm. Thus, the combined SAXS/DIC techniques cover both the large-scale structure of liposome aggregates (sub- to many 10s of μm) and the length scale of liposome–liposome tethering due to DEA-PEG. The key length-scale of interest is that of the membrane wall-to-wall separation distance, which corresponds to q>0.04 Å^{-1} in the SAXS data.

The liposome suspensions were loaded into quartz capillaries and centrifuged gently (10,000 g) immediately prior to measurement to concentrate the liposomes and aggregates near the bottom of the capillary. Sonicated liposomes are typically <300 nm in diameter, resulting in transparent solutions. In contrast, Mie scattering by objects with sizes around or larger than the wavelength of visible light (>380 nm) gives the suspension a gray or white (opaque) appearance. Thus, solution opacity may (with limitations) serve as a semiquantitative indicator of liposome aggregation (by tethering or membrane

fusion) after sonication. The observed turbidity of our samples containing DEA-PEGs (see Figure S3 in the Supporting Information) is suggestive of liposome–liposome tethering by DEA-PEGs. However, the observed turbidity may also be due to other fluctuation effects, e.g., large vesicle shape fluctuations which will also appear as a bluish color of the suspension. The SAXS data described below, for increasing contents of DEA-PEG, show clear evidence of bridging between neighboring membranes. In particular, the SAXS analysis of liposomes containing 5 and 10 mol% DEA-PEG shows that the membrane wall-to-wall spacing is of order the radius of gyration of the PEG tether for both PEG2000 and PEG4600.

Figure 6 shows the SAXS profiles for control liposomes with 10 mol% PEG-lipid (SEA-PEG with no tethering functionality; dashed line profiles in panels A,B,C), and liposomes with increasing DEA-PEG content (solid colored lines at 2, 5, and 10 mol%), for neutral liposomes without DOTAP (panels A and B) and cationic liposomes with 10 mol% DOTAP (panel C). All SAXS profiles show the form factor associated with lipid membranes, with minima around q=0.03 to 0.04 Å^{-1} and slightly larger than 0.2 Å^{-1}. Broad peaks are visible in most profiles, indicating short-range intermembrane correlations of the lipid membranes.

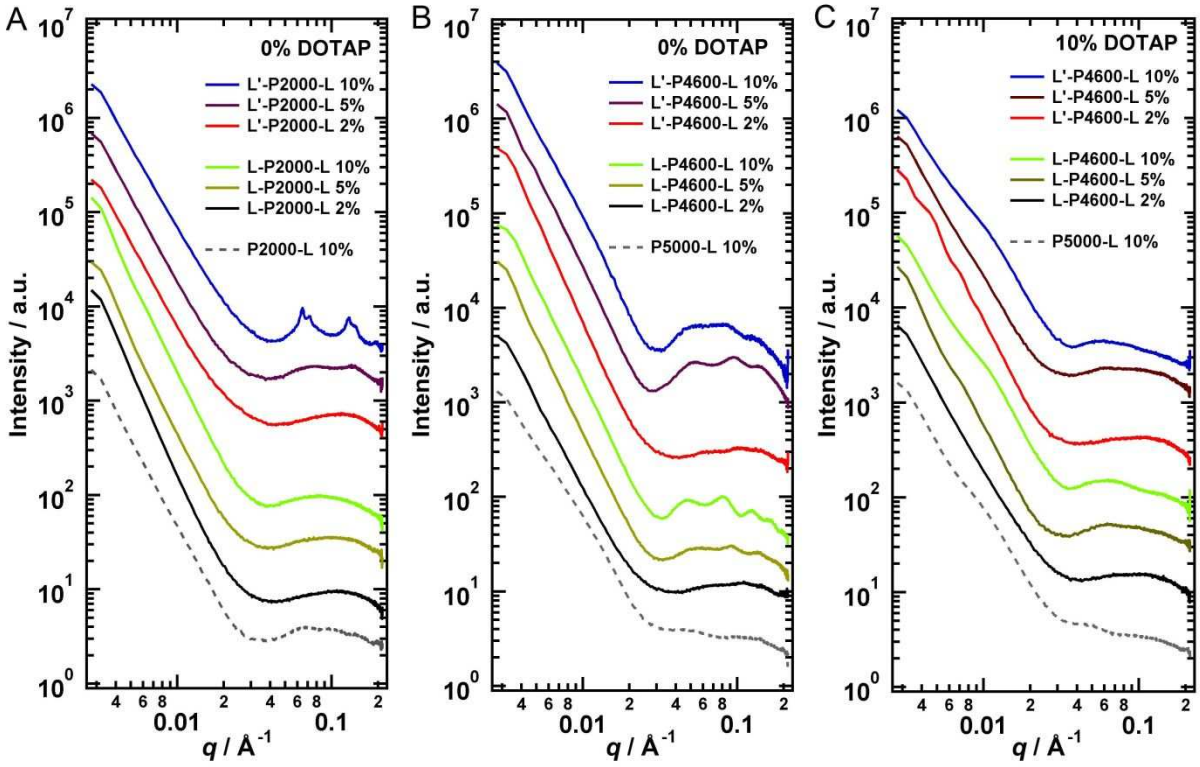

Figure 6. Small-angle X-ray scattering profiles of suspensions of neutral (0% DOTAP) and cationic (10% DOTAP) DOPC/DEA-PEG liposomes and controls. Profiles were selected from a region near the bottom of the capillaries, where denser samples (formed by centrifugation) produced stronger scattering signals. (A)

SAXS profiles from samples containing liposomes with increasing concentrations (2, 5, and 10 mol%, respectively) of symmetric (L-P2000-L) and asymmetric (L'-P2000-L) DEA-PEG2000 and no DOTAP. The SAXS profile from a control sample containing 10 mol% of the corresponding SEA-PEG (P2000-L) is also shown (grey dashed line). (B) SAXS profiles from samples containing liposomes with increasing concentrations (2, 5, and 10 mol%, respectively) of symmetric (L-P4600-L) and asymmetric (L'-P4600-L) DEA-PEG4600 and no DOTAP. The SAXS profile from a control sample containing 10 mol% of the corresponding SEA-PEG (P5000-L) is also shown (grey dashed line). (C) SAXS profiles from samples containing cationic liposomes with 10 mol% DOTAP and increasing concentrations (2, 5, and 10 mol%, respectively) of symmetric (L-P4600-L) and asymmetric (L'-P4600-L) DEA-PEG4600. All samples containing DEA-PEGs other than L-P2000-L show multiple broad peaks in the scattering profiles, which indicates correlations between membranes. See the text for detailed discussion.

The control samples prepared with PEG-lipids (SEA-PEG; dashed gray lines in Figure 6) show two very weak, broad correlation peaks, indicating weakly correlated membranes with small coherent domains. The existence of the broad peaks signifies some weak intermembrane correlations, possibly because a fraction of the PEG-lipid phase-separates into micelles, which would exert depletion-attraction forces on the liposomes. The peak positions are different for the two PEG lengths, with longer PEG resulting in a peak at smaller q (larger d; compare dashed profiles in panels B and C with the dashed profile in panel A). Interestingly, the values of d calculated from the SAXS profiles are close to those for the DEA-PEGs (see discussion below), further suggesting that the size of the PEG chains is an important parameter in determining organization of the liposomes.

Turning to Figure 6A for neutral liposomes containing DEA-PEG with shorter (2000 g/mol) PEG chains, the SAXS profiles of the samples containing the symmetric DEA-PEG (L-P2000-L) appear to show only the liposome form factor at the length scales investigated ($2\pi/q \approx 30$ to 2500 Å), with little to no evidence of any correlation peaks (panel A, 2nd through 4th profiles from bottom for 2, 5, and 10 mol% DEA-PEG). In a previous study of bulk multilamellar lyotropic lipid phases, L-P2000-L exhibited slower kinetics than all the other DEA-PEGs, requiring between one and two months to reach equilibrium with clear onset of the bridging conformations at 5 mol% DEA-PEG.[50] In the present work, SAXS of the samples of dilute suspensions of neutral liposomes in excess water was measured within a week of lipid hydration and sonication. While this means that the samples containing L-P2000-L would likely eventually show ordered membranes and aggregation (as also observed in DIC for cationic liposomes at low membrane charge density), it is irrelevant for practical applications that would require tethering to take place on a shorter time scale.

Significantly larger correlation peaks were observed in samples containing increasing concentrations of the asymmetric DEA-PEG (L'-P2000-L) at 2, 5, and 10 mol%. (Figure 6A, top three profiles). The

presence of one less hydrophobic anchor lowers the energetic barrier for switching between the looping and bridging conformations (Figure 2B), which is the likely cause of the faster kinetics previously observed for this DEA-PEG compared to its symmetric counterpart.[50] The SAXS profile at 10 mol% L'-P2000-L (Figure 6A, top profile) shows evidence of two coexisting lamellar phases, with visible first and second harmonics for each phase, at lamellar membrane spacings of 97.6 and 87.4 Å. This is consistent with membrane–membrane bridging as described in more detail below.

Focusing on the long DEA-PEGs with PEG molecular weight 4600 g/mol, the samples containing symmetric L-P4600-L (Figure 6B, 2nd to 4th profiles from bottom) show increasingly stronger correlation peaks as the concentration of DEA-PEG increased from 2 mol% to 10 mol%. In particular, the sample with 10 mol% DEA-PEG showed four strong correlation peaks. The SAXS profiles for the asymmetric DEA-PEG (L'-P4600-L) are qualitatively similar, with those at 5 and 10 mol% DEA-PEG displaying three weak correlation peaks (Figure 6B, top two profiles). Importantly, the correlation peaks are significantly stronger and narrower than the peaks for the sample containing the control PEG-lipid (SEA-PEG; P5000-L) which confers repulsive intermembrane interactions (gray profile in Figure 6B). These stronger peaks indicate increased correlations resulting from intermembrane bridging due to the presence of the DEA-PEG (see Figure 7 for lineshape analysis).

Figure 6C shows SAXS profiles for cationic liposomes with 10 mol% DOTAP as a function of increasing content of symmetric (L-P4600-L, 2nd,3rd,4th profile from bottom) and asymmetric (L'-P4600-L, top three profiles) DEA-PEG (2, 5, and 10 mol%). As evident from small changes in the scattering profiles, the correlations that set in as the DEA-PEG content increases from 2 to 5 and 10 mol% are modest. This is due to the added intermembrane electrostatic repulsion conferred by the addition of 10 mol% of cationic DOTAP, which competes with and weakens the attractive interactions resulting from the DEA-PEG. Nevertheless, it is important to note that the position of the broad correlation peak that sets in at around $q \approx 0.057$ Å^{-1} is very close to that ($q \approx 0.05$ Å^{-1}) of the first sharper correlation peak which sets in for the neutral liposomes (compare, for example, the lowest-q peaks for the sample at 10 mol% L-4600-L in panel B and the sample at 10 mol% L-4600-L in panel C; see also Figure 7). Thus, intermembrane bridging is still present in cationic liposomes but much weaker than in neutral liposomes.

To further clarify the nature of the broad correlation peaks observed in SAXS, we carried out least-square fits of the data to Lorentzian-shaped structure factor peaks. The broad peaks in the SAXS profiles indicate short-range intermembrane positional correlations with density–density correlations that decrease exponentially as $(1/r)\times\exp(-r/L_C)$, with L_C the intermembrane correlation length or, equivalently, the coherent domain size. Thus, we would expect the X-ray structure factor, which is proportional to the Fourier transform of the density–density correlation function, to be described by a Lorentzian function.[62] For each peak the Lorentzian function was written as $S(q) = A/[(q-q_0)^2+\kappa^2]$. The fitting parameters were

q_0, κ, and A with q_0 the peak position (in Å^{-1}), κ the half-width-at-half-maximum (HWHM; in Å^{-1}) and A/κ^2 the peak intensity. The interlayer spacing d then is $d=2\pi/q_0$, and the coherent domain size (L_C) is given by the inverse of the HWHM, $L_C = 1/\kappa$.

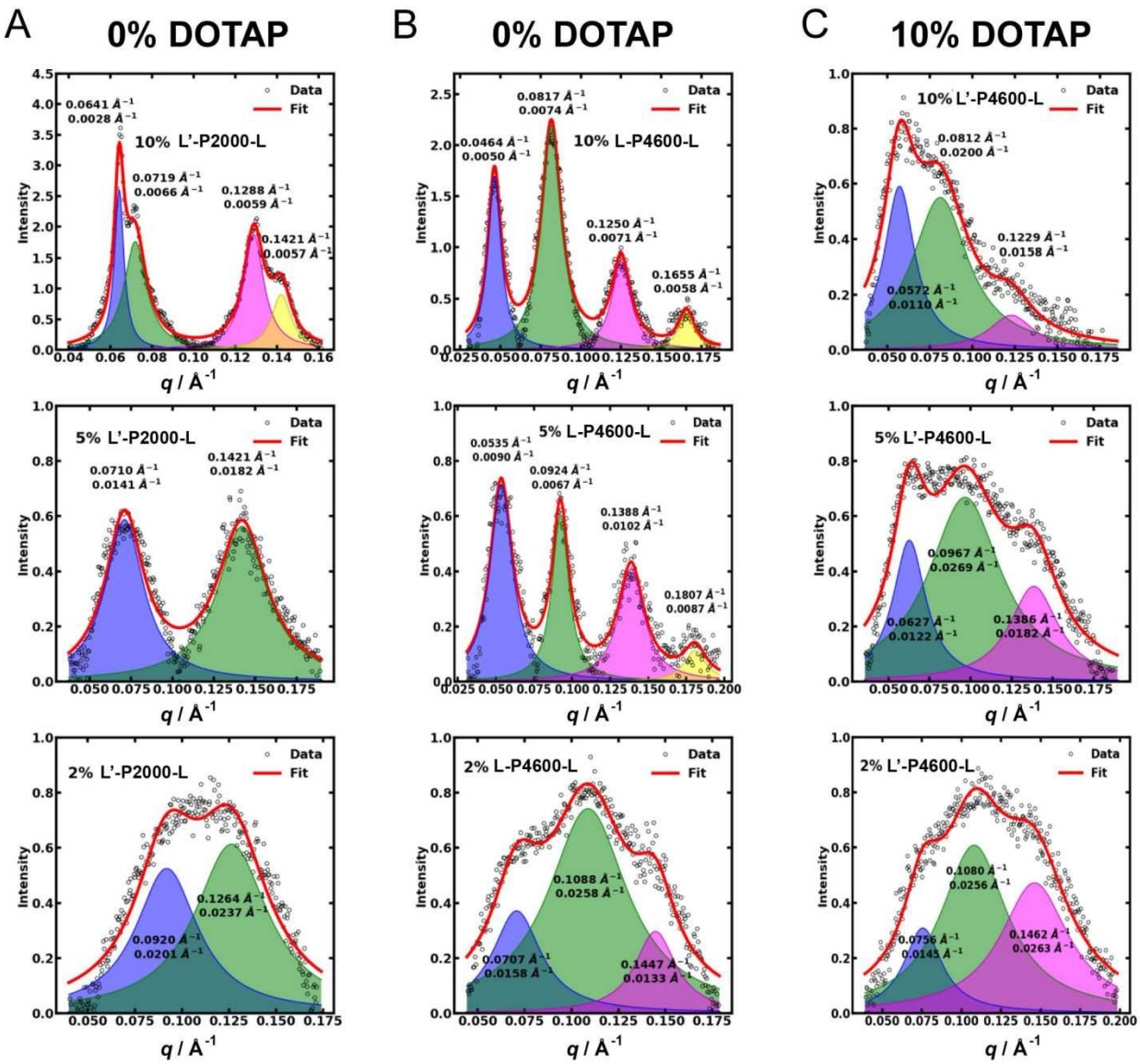

Figure 7. Fits of selected SAXS profiles with model Lorentzian-shaped structure factor peaks arising from short-range intermembrane correlation. The data was fit after background subtraction. The profiles are a subset of the data shown in the corresponding panels (A,B,C) in Figure 6. The q-range of the data shown and fitted corresponds to the length-scale at which intermembrane correlations were expected. The parameters shown for each fitted peak are the peak position (top) and half-width at half-maximum (HWHM, bottom), respectively. (A) Fitting of the intermembrane correlation peaks for samples of neutral DOPC liposomes (no DOTAP) incorporating asymmetric L'-P2000-L DEA-PEG at increasing

concentrations (from bottom to top: 2, 5, and 10 mol%). With increasing DEA-PEG concentration the peaks become stronger and sharper, indicating enhancement of intermembrane order by DEA-PEG-induced bridging. (B) Peak fitting for neutral DOPC liposomes incorporating symmetric L-P4600-L DEA-PEG at 2, 5, and 10 mol% (from bottom to top). Again, the results demonstrate that the intermembrane ordering increases with increasing amount of DEA-PEG. (C) SAXS peak fitting for cationic liposomes (DOPC and 10 mol% DOTAP) incorporating asymmetric L'-P4600-L DEA-PEG at 2, 5, and 10 mol% (from bottom to top). The peaks for these samples are weaker and broader than those observed for neutral liposomes due to electrostatic repulsion. However, the trend that the intermembrane ordering increases with increasing amount of DEA-PEG holds.

Figure 7 shows examples of fits of the model (solid red lines, representing the sum of the individual Lorentzian functions that are shown as filled-in curves) to the background-subtracted SAXS data (open circles) of Figure 6. It is apparent that Lorentzian line-shapes, representing short-range intermembrane correlations, fit the data well. Each panel also lists the peak position (q) and the HWHM (κ) of the individual Lorentzian functions. Figure 7A depicts fits of Lorentzian functions to the SAXS data for neutral liposomes containing asymmetric (L'-P2000-L) DEA-PEG at 2, 5, and 10 mol%. At 5 mol% (middle plot), the SAXS data fits to a sum of two Lorentzian functions, which index as the first and second harmonics (with peaks at q_{001} and q_{002}) of a lamellar phase with interlayer spacing $d=2\pi/q_{001}=88.5$ Å and with weak near-neighbor correlation lengths ($1/\kappa$) between 55 Å and 71 Å as determined from the widths of the Lorentzian functions. Considering that the membrane bilayer thickness is $d_m\approx40$ Å, the wall-to-wall spacing between two membranes with $d=88.5$ Å is $d-d_m\approx48.5$ Å, comparable to the intermembrane correlation length. In contrast, Figure 7A (top plot) depicts fits of Lorentzian functions to the sharp peaks observed for the sample at 10 mol% L'-P2000-L which reveal two coexisting lamellar domains. Each of these exhibit strong first and second harmonics, with membrane spacings d of 97.6 Å and 87.4 Å ($q_{001}=0.0641$ and 0.0719 Å^{-1}), respectively. In this sample the correlation length (or lamellar coherent domain size) varies between ≈167 Å (1/0.0066 Å^{-1}) and 357 Å (1/0.0028 Å^{-1}), i.e., between 2 to 4 layers. The two Lorentzian functions that fit the data of the sample with only 2 mol% L'-P2000-L (Figure 7A, bottom plot) are much broader than those for the samples containing 5 and 10 mol% DEA-PEG, with very weak intermembrane correlations ($1/\kappa\approx1/0.02$ Å$^{-1}=50$ Å). Furthermore, the broad peaks indicate a distribution of interlayer spacings d between 49.7 Å and 68.3 Å. Thus, the SAXS data shows progressively enhanced intermembrane correlations and a much narrower distribution of interlayer spacings (with d between 87.4 Å and 97.6 Å) as the DEA-PEG concentration increases from 2 to 5 and 10 mol%, strongly suggesting that these correlations result from DEA-PEG-mediated bridging. As expected for membranes tethered by PEG, the interlayer spacings correspond to membrane wall-to-wall spacings ($d-d_m\approx47.4$ Å and 57.6 Å) that are comparable to, but larger than, the radius of gyration of the PEG tether

with molecular weight 2000 g/mol ($R_G \approx 35.3$ Å). Remarkably, the spacings in the samples containing 5 and 10 mol% L'-P2000-L are in very good agreement with the range of spacings found for bulk (very high lipid concentration) repulsive (cationic) lamellar phases containing symmetric and asymmetric DEA-PEGs of PEG molecular weight 2000 g/mol in the presence of excess water (d≈85–100 Å).[50]

Figure 7B shows examples of fits to the SAXS profiles of neutral liposomes containing increasing amounts of symmetric long DEA-PEG (L-P4600-L). The broad profile of the sample containing 2 mol% DEA-PEG may be fit to three broad Lorentzian functions, indicating a distribution of interlayer spacings d between ≈58 Å and ≈89 Å. The broad peaks due to weak intermembrane correlations are similar to those from the sample with 2 mol% L'-P2000-L (Figure 7A, lower plot), but the distribution of interlayer spacings is shifted to larger values, as would be expected upon increasing the PEG molecular weight from 2000 to 4600 g/mol. At increased DEA-PEG concentrations of 5 mol% (Figure 7B, middle plot) and 10 mol% (Figure 7B, top plot), the SAXS data show more well-defined peaks indicative of DEA-PEG-mediated bridging. The data at both DEA-PEG concentrations is fit well by the sum of four Lorentzian functions, which can be indexed to a single lamellar phase with four harmonics (00L, L=1,2,3,4) at peak positions $q_{00L} = Lq_{001}$. While the second through forth peak positions agree precisely with integer indexing of a phase with lamellar symmetry (with $q_{002} = 0.092$ Å^{-1} and 0.082 Å^{-1} for 5 and 10 mol%, respectively), the first harmonic (q_{001}) is slightly shifted to higher q compared to the second, third, and fourth harmonics. This is most likely due to a shift of this peak resulting from the nearby form factor minimum at q≈0.04 Å^{-1} (see profiles in Figure 6). For these samples at 5 and 10 mol%, the interlayer spacing is d=136 Å and d=153 Å, respectively, as measured from the second harmonic ($d = 2(2\pi/q_{002})$). Thus, the membrane wall-to-wall spacings of $d–d_m$=96 Å and 113 Å for 5 and 10 mol%, respectively, are again comparable to (but larger than) the radius of gyration of the PEG4600 tether (R_G≈62 Å). The correlation lengths (or lamellar coherent domain sizes) varied between ≈100 Å and 149 Å (1/0.01 Å^{-1} and 1/0.0067 Å^{-1}) for 5 mol% DEA-PEG and ≈ 135 and ≈ 172 Å (1/0.0074 Å^{-1} and 1/0.0058 Å^{-1}) for 10 mol% DEA-PEG. This implies near-neighbor intermembrane correlations when taking into account the membrane thickness d_m≈40 Å. As in the case of the shorter PEG, the found intermembrane spacings are consistent with those found for bulk repulsive (cationic) lamellar phases that exhibited DEA-PEG bridging in the presence of excess water (≈130 Å).[50]

Figure 7C depicts fits to SAXS data of cationic liposomes containing 10 mol% DOTAP and 2, 5, and 10 mol% asymmetric (L'-P4600-L) DEA-PEG. The SAXS data for the sample at 2 mol% DEA-PEG (Figure 7C, bottom plot) is qualitatively similar to that for neutral liposomes at the same concentration of the symmetric (L-P4600-L) DEA-PEG (Figure 7B, bottom plot), displaying a very broad feature in the SAXS profile for which fits to three Lorentzian functions the give a distribution of interlayer spacings between d≈58 Å and d≈83 Å. Interestingly, the first Lorentzian peak is noticeably enhanced as the DEA-

PEG content increases, with $d=2\pi/0.0627$ Å^{-1})≈100 Å and $d=2\pi/0.0572$ Å^{-1}≈110 Å at 5 and 10 mol%, respectively, and narrower peak widths indicating near-neighbor intermembrane correlations. The peaks are overall very broad compared to those observed in the SAXS profiles from neutral liposomes at 5 and 10 mol% symmetric (L-P4600-L) DEA-PEG (Figure 7B, middle and top plots). This shows that the electrostatic repulsion between neighboring membranes, introduced by inclusion of charged DOTAP, competes with attractions mediated by DEA-PEG bridging and leads to much weaker intermembrane correlations.

The combined SAXS data, including the quantitative line-shape analysis of X-ray profiles as a function of increasing concentrations of DEA-PEG, demonstrates bridging between neighboring membranes with membrane wall-to-wall spacing comparable to the radius of gyration of the PEG tether for both PEG2000 and PEG4600.

Cryogenic Transmission Electron Microscopy (Cryo-EM)

While SAXS provides ensemble-averaged information about a sample's nanostructure, real-space imaging can be useful to reveal examples of representative structures. Thus, we performed cryogenic transmission electron microscopy (cryo-EM) with selected lipid-based systems with and without DEA-PEGs (see Figure 8).

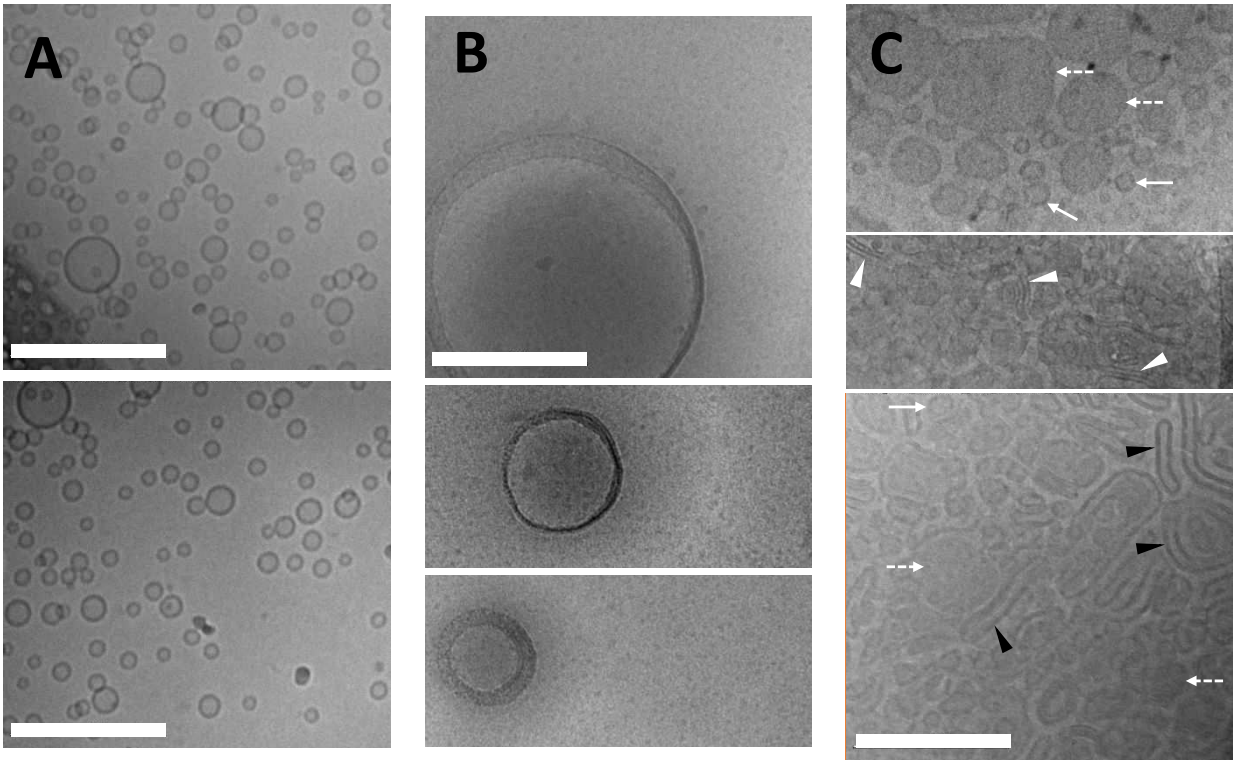

Figure 8. Representative cryogenic electron micrographs of suspensions of neutral lipid with (B) and without (A) DEA-PEG and of cationic liposome–DNA (CL–DNA) complexes formed from CLs containing DEA-PEG (C). (A) The neutral lipid mixture without PEG-lipid (97/3 DOPC/paclitaxel, mol/mol) forms small, unilamellar liposomes after sonication. (B) No small liposomes are observed in a sample containing 10 mol% of the DEA-PEG L'-P2000-L in addition to DOPC. Instead, the micrographs show larger, circular and near-circular structures with thick shells. The contrast and thickness of the shells vary, even within a single structure. (C) CL–DNA complexes were formed by mixing (anionic) DNA with liposomes containing DOTAP/DOPC/L-P4600-L at a 30/65/5 molar ratio. Cryo-EM reveals liposomes (objects with darker outline; solid arrows) as well as CL–NA NPs (dashed arrows). Notably, the images also show membrane structures with a constant interlamellar distance of ≈7 nm (white arrowheads) and ≈13 nm (black arrowheads). These distances are identical to the interlamellar distance of lamellar DOTAP/DOPC–DNA complexes determined by SAXS[63] (7 nm) and the tethering distance (13 nm) observed in the SAXS measurements reported in this work as well as in bulk (very high lipid concentration) samples of cationic membranes containing L-P4600-L or L'-P4600-L.[50] Scale bars: 200 nm.

The neutral liposomes (Figure 8A; composed of 97/3 DOPC/paclitaxel) were prepared by sonication and frozen within two days, preventing significant aggregation through van der Waals interactions. Cryo-EM imaging reveals small, unilamellar liposomes with diameters between 10 and 100 nm.

Cryo-EM imaging detected no small unilamellar liposomes in the sample of neutral (DOPC) liposomes containing 10 mol% L'-P2000-L (Figure 8B). The only objects revealed by cryo-EM are larger, circular and near-circular shell-like objects with diameters ranging from 30 nm to nearly 400 nm. The walls of these objects vary in thickness and contrast in the micrographs and are distinct from the single membranes of the control neutral liposomes. Some but not all of the walls resemble concentric lipid membranes.

It is important to remember that cryo-EM is unable to image all the structures present in the sample because of the technique's limitations for large aggregates. However, the large effect on the structure and assembly of neutral liposomes that incorporating a DEA-PEG has is evident from the data in the large differences with the control sample, which are consistent with aggregate formation. Also notable is that the observed structures formed in less than three days (the time elapsed between sonication and vitrification). This is in contrast to samples of bulk lamellar phases (at very high lipid concentration) containing DEA-PEGs, which require equilibration times on the order of weeks to months.[50]

To gain further insight into the structures formed by incorporation of DEA-PEGs into lipid membranes with cryo-EM, we prepared cationic liposome–DNA nanoparticles (CL–DNA NPs) by mixing sonicated, cationic liposomes containing 5 mol% L-P4600-L (as well as 30 mol% cationic DOTAP and the remainder DOPC) with a solution of (anionic) DNA at a slightly positive CL/DNA charge ratio of ρ=1.25. The structure of CL–DNA NPs after the addition of SEA-PEG (PEG-lipid) has previously been

studied.[31,32] In preparations with excess cationic lipid (i.e., ρ>1), CL–DNA NPs coexist with excess cationic liposomes and threadlike micelles containing PEG-lipid.[31]

Cryo-EM imaging of the DEA-PEG-containing CL–DNA NP sample (Figure 8C) shows several main features. One of these are small unilamellar liposomes (solid arrows). The electrostatic repulsion introduced by the presence of cationic lipid in the membrane likely is one factor that leads to some liposomes remaining (other than in the sample of DEA-PEG-containing neutral liposomes (Figure 8B)). In contrast to samples containing SEA-PEGs,[31] no threadlike micelles were observed.

Another prominent feature in Figure 8C are larger objects with little to no contrast between the outer shell and inside (dashed arrows; diameter ~ 50–150 nm). This means that these objects are not hollow liposomes but likely CL–DNA NPs with little or no discernable internal structure. They may lack internal structure because the structure has not yet reached equilibrium, because these are lamellar structures viewed top-down, or because the presence of the DEA-PEG promotes a less ordered internal structure. At the same time, the images also show structures with a constant interlamellar distance of ~7 nm (white arrowheads), identical to the interlamellar distance of lamellar DOTAP/DOPC–DNA complexes determined by SAXS.[63]

Remarkably, the micrographs also show several membrane structures with a constant distance of ~10 – 13 nm (black arrowheads). This is identical to the tethering distance observed in the SAXS measurements in the current work and in bulk samples of cationic membranes (at very high lipid concentrations) doped with L-P4600-L and L'-P4600-L.[50] Thus, these uniformly-spaced structures likely represent membranes tethered by the DEA-PEG. There is additional evidence for aggregation in the lower- and intermediate-resolution electron micrographs (see Figure S4 in the Supporting Information). These show material (which consists of the features mentioned above) that appears to be connected and is spread across and on top of several of the holes in the lacey carbon grid.

Confocal Microscopy of CL–DNA NPs and Rab Proteins in Cells

To assess whether DEA-PEGs are also able to affect assembly of lipid-based building blocks inside of cells, we turned again to CL–DNA NPs. The controls without PEG-lipid and with SEA-PEG have been characterized extensively: while CL–DNA complexes without PEG-lipid tend to form large aggregates in cell culture medium, addition of PEG-lipid (SEA-PEG) generates small, stable NPs that, however, show weaker attractive interactions with cellular membranes due to the steric repulsion of the PEG corona.[32-34] This repulsion can be modulated and overcome by increasing NP charge,[34,38,39] triggering the release of the PEG chain inside endosomes that undergo acidification,[33] or adding a receptor-binding moiety on the distal end of the PEG.[34,39] Here, we sought to determine whether the addition of a hydrophobic moiety to

a PEG-lipid (i.e., the second "anchor" of the DEA-PEG) can also promote binding to the plasma membrane, affect endocytosis by cells, or modulate interactions with internal cellular membranes.

PEGylated CL–DNA NPs enter cells via endocytosis, leading to initial NP entrapment inside early endosomes.[57] The early endosomes containing NP cargo then undergo intracellular trafficking through distinct pathways.[64] This vesicle trafficking between organelles is highly regulated, in particular by the Rab proteins, a family of small GTPases in eukaryotes.[65-67] Figure 9 schematically shows the roles of various Rab GTPases in early endosome (Rab5), late endosome (Rab7, Rab9)/lysosome (Rab7), and recycling endosome (Rab4; Rab11) trafficking.

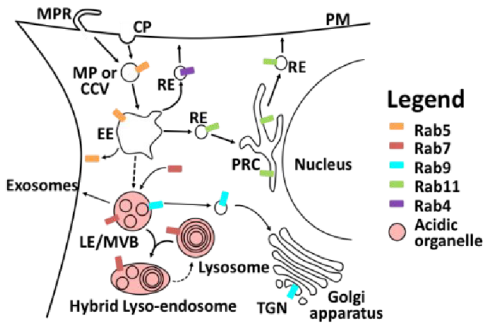

Figure 9. Rab-family proteins as modulators and markers of the late endosome/lysosome and fast (Rab4) and slow (Rab11) endosomal recycling pathways. Adapted with permission from reference[38]. Copyright 2016 American Chemical Society. (CCV: clathrin-coated vesicles; CP: clathrin pits; EE: early endosome; LE: late endosome; MP: macropinosomes; MPR: macropinocytic ruffles; MVB: multivesicular body; PM: plasma membrane; PRC: perinuclear recycling center; TGN: trans-Golgi Network.)

To visualize CL–DNA NPs on distinct intracellular pathways, we employed confocal microscopy of PC-3 cells incubated with NPs containing DEA-PEGs and DNA that was covalently labeled with a fluorescent dye (Cy5). To label endosomal pathways, the cells were transfected to express GFP-conjugated Rab11 and treated with LysoTracker. Rab11 is associated with the (slow) recycling endosomal pathway, and LysoTracker is a commercial dye that labels acidic organelles and has been shown to colocalize with Rab7 and Rab9 (i.e., late endosome and lysosomes (Figure 9)).[38]

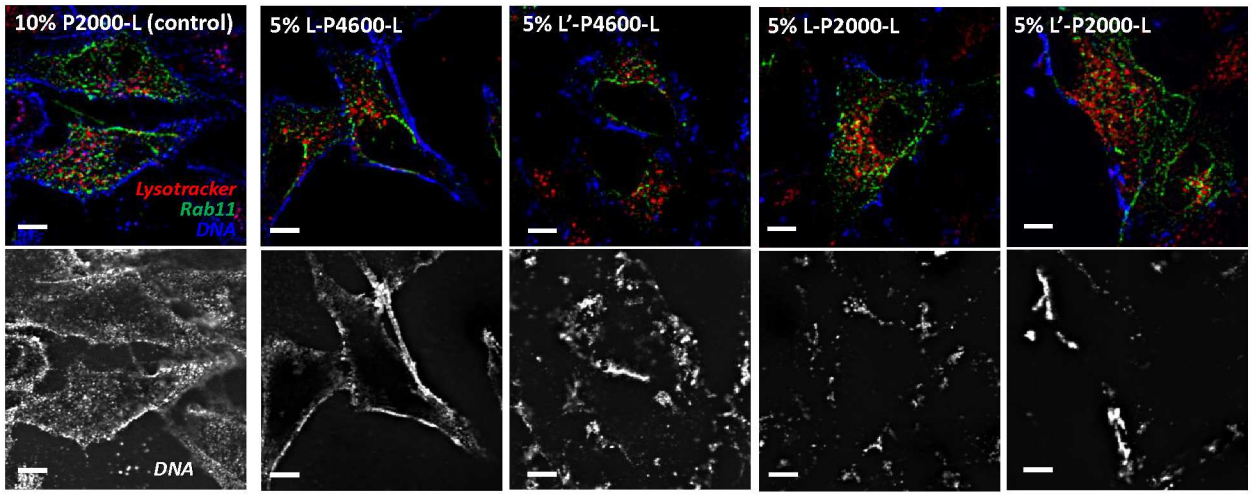

Figure 10. Confocal micrographs (representative z-slices) of PC-3 cells incubated with CL–NA NPs containing SEA-PEG or DEA-PEG. NPs were prepared from cationic liposomes of a molar composition of 10/80/10 MVL5/DOPC/P2000-L (control) or 11/84/5 MVL5/DOPC/DEA-PEG at a CL/DNA charge ratio of ρ=5 (closely mimicking the composition of previously studied[38] CL–DNA NPs with peptide-PEG-lipids). (Top) Colored images showing DNA (blue; Cy5 label) and the Rab11/recycling (green; GFP) and late endosome/lysosomes (red; Lysotracker) endosomal pathways. (Bottom) Images showing only the Cy5 (DNA) channel (without coloring) of the same micrographs to facilitate assessing the distribution of the labeled CL–DNA NPs. NPs containing DEA-PEGs appear to form aggregates, with many of the larger aggregates remaining attached to the cell surface and little internalization by the PC-3 cells. Scale bars: 10 μm.

The top part of Figure 10 displays representative color images of three-channel, fluorescent confocal micrographs (representative z-slices) of cells, with endosomal pathways in green (Rab11/recycling pathway) and red (Lysotracker/late endosome–lysosome pathway) and CL–DNA NPs in blue. Typically, CL–DNA NPs are visible both within the cell and without (outlining the plasma membrane). The cells were incubated with CL–DNA NPs containing either SEA-PEG (control; 10 mol% P2000-L) or one of the DEA-PEGs (5 mol% DEA-PEG). Below the color images are images showing only Cy5 fluorescence (i.e., DNA), to more clearly reveal the location of CL–DNA NPs within the cell.

The point-like particles of the control (SEA-PEG) sample outline most of the cell and are dispersed evenly throughout most of the interior of the cell (excluding the nucleus, which can be distinguished in the color images by the absence of red or green (endosomal) labels). In contrast, the particles containing DEA-PEGs mostly appear to form large aggregates. Of these samples, the one containing L-P2000-L showed the least prevalence of large aggregates, which is consistent with our findings in the SAXS and imaging experiments with liposome suspensions. All the DEA-PEG-containing samples show a significantly decreased number of CL–DNA particles within the cell boundary compared to the control,

with most particle aggregates stuck to the surface of the cell. The few particles that are internalized by the cells are smaller than the typical aggregates.

These results again demonstrated the ability of DEA-PEGs to aggregate lipid-based building blocks. However, the aggregation appeared to limit uptake by cells and thereby our ability to assess the effect of DEA-PEGs on intracellular membranes and pathways. We thus prepared CL–DNA NPs containing a slightly reduced amount of DEA-PEG and additional SEA-PEG, applying the earlier finding that repulsive steric interactions from the SEA-PEG would temper the attractive interactions mediated by the DEA-PEGs and reduce aggregation.

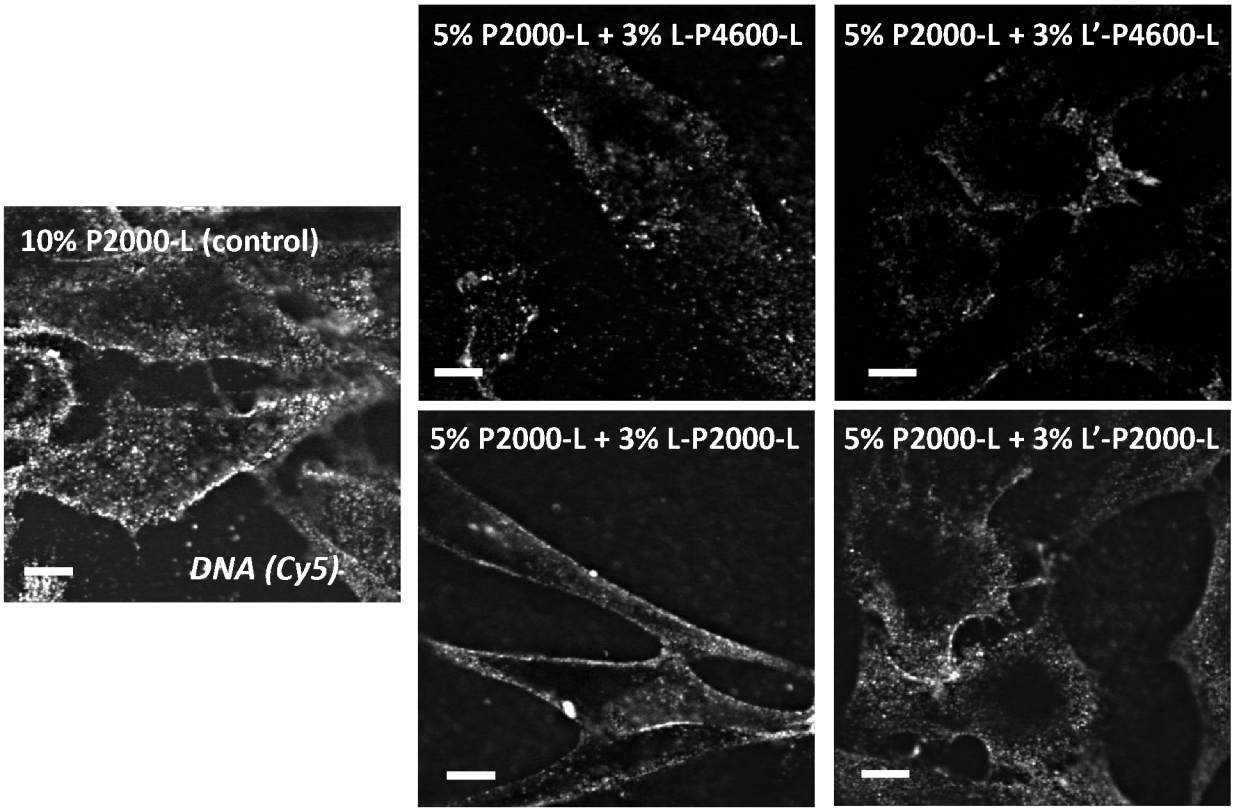

Figure 11. Confocal micrographs (representative z-slices) of PC-3 cells incubated with CL–NA NPs containing SEA-PEG only (control) or a mixture of DEA-PEG and SEA-PEG. To facilitate assessing the distribution of the labeled NPs, only the Cy5 (DNA) channel (without coloring) is shown. CL–NPs were prepared from cationic liposomes of a molar composition of 10/80/10 MVL5/DOPC/P2000-L (control) or 10/82/5/3 MVL5/DOPC/P2000-L/DEA-PEG, at a CL/DNA charge ratio of ρ=5. The steric-stabilization conferred by the additional SEA-PEG reduced aggregation and increased internalization by the PC-3 cells compared to similar NPs prepared with only DEA-PEG (Figure 10). Scale bars: 10 μm.

Figure 11 displays representative micrographs (representative z-slices; Cy5/DNA channel only) of CL–DNA NPs containing 5 mol% SEA P2000-L and 3 mol% DEA-PEG. The images show a smaller average

size of the CL–DNA NPs and reduced formation of large aggregates. In addition, the NPs are distributed more evenly instead of mostly outlining the exterior boundary of the cells; a larger fraction of them is internalized by the cells (albeit still at a lower number than the control SEA NPs). This shows that tuning of the attractive interactions mediated by the DEA-PEGs by added steric repulsion (SEA-PEG) can also be achieved in the context of CL–NA NPs.

Colocalization analysis of CL–DNA NPs with endosomal pathways

To quantify the information from the confocal microscopy experiments, we used object-based colocalization analysis.[38,51,57] The software first identifies the positions of CL–DNA NPs and labeled endosomal vesicles within the cell and then determines whether these positions are close enough for the NPs to be considered associated with the labeled endosomal pathways. This process is illustrated in Figure 12A; the micrograph shows labeled late endosome/lysosome (Lysotracker, red) and recycling endosome (Rab11, green) vesicles as well as labeled CL–DNA NPs (blue). A profile of the intensities of the three fluorescent channels along the dotted white line in the micrograph is plotted in Figure 12B. The three distinct peaks in the Cy5/DNA channel (blue line) indicate the location of three distinct NPs. The first peak (i) coincides with a peak in the Lysotracker channel (red line), and the third peak (iii) closely overlaps with a peak in the Rab 11 channel (green line). Thus, the corresponding CL–DNA NPs would be categorized as being colocalized with the late endosome/lysosome (i) and the Rab11 recycling pathway (iii), respectively. The second peak (ii) does not significantly overlap with peaks in either the red or green channel and the corresponding NP would be categorized as colocalized with neither pathway. NPs associated with neither pathway may be located in the cytoplasm of the cell (having either escaped an endosome via membrane fusion or fused directly with the plasma membrane) or could be associated with another endosomal pathway or organelle that has not been fluorescently labeled.

The results of the quantitative colocalization analysis with recycling endosomes (Rab11) and acidic organelles (Lysotracker) are summarized in Figure 12, parts C–F. Data for the control CL–DNA NPs containing only SEA-PEG (P2000-L) are shown in gray. Results for the CL–DNA NPs containing 5 mol% DEA-PEGs (and no SEA-PEG) are shown in Figure 12, parts C and D. Because too few CL–DNA NPs containing short-chain DEA-PEGs (L/L'-P2000-L) were identified within the cells to obtain statistically significant results, no data is shown for these DEA-PEGs. For the longer-chain DEA-PEGs, the number of particles counted per cell is still low (at ~20-40% of the counts) relative to the SEA-PEG control (Figure 12D), indicating the effect of particle aggregation. For both samples, colocalization of NPs (Figure 12C) with the late endosome/lysosome pathway dropped relative to the SEA control by 7 to 9% of internalized NPs (≈half the level of the control), while colocalization with the Rab11 recycling pathway remained constant (≈23 to 25% of internalized NPs). Meanwhile, the fraction of particles that

were colocalized with neither pathway was significantly higher (by 13 to 16% of internalized NPs) over the SEA-PEG control (to a level ≈1.3-fold of the control).

We repeated the quantitative colocalization measurements with NPs that were partially stabilized by 5 mol% SEA-PEG P2000-L in addition to containing 3 mol% DEA-PEGs (see also Figure 11). All these NPs were internalized by the cells at numbers sufficient to obtain adequate colocalization data. However, the number of DNA-containing NPs within the cell boundary (Figure 12F) for these formulations was still significantly lower than that for the SEA-PEG NPs (roughly 30-60% of the control). In contrast to NPs containing DEA-PEG but not SEA-PEG, only the NPs with asymmetric DEA-PEGs (L'-P4600-L and L'-P2000-L) exhibited significantly changed colocalization patterns. CL–DNA NPs containing L'-P4600-L showed the most dramatic shift, with Lysotracker colocalization dropping to 33% and colocalization with neither pathway increasing to 140% of the control. Similarly, for NPs containing L'-P2000-L, Lysotracker colocalization dropped to ~60% and colocalization with neither pathway increased to 120% of the control. There was no significant change in colocalization with Rab11 for any of the DEA-PEG-containing NPs.

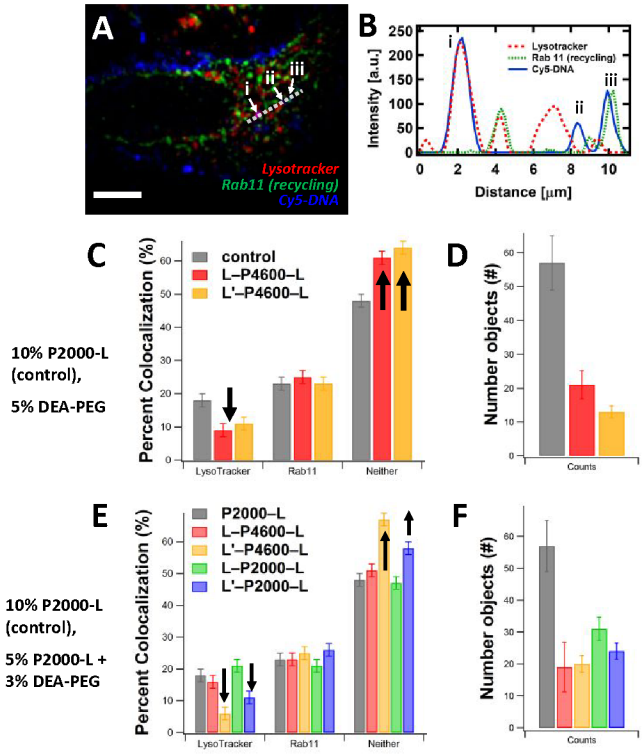

Figure 12. Colocalization of DEA-PEG-containing CL–DNA NPs with the late endosome/lysosome (LysoTracker) and recycling (Rab11) endosomal pathways in PC-3 cells from multi-organelle fluorescence imaging. (A) Example confocal micrograph of a cell with fluorescently-labeled Rab11 recycling (green; GFP) and late endosome/lysosome pathways (red; Lysotracker) after treatment with CL–DNA NPs

containing labeled DNA (blue; Cy5). (B) Profiles of the three fluorescence channels along the dotted line in part A. Three objects (labeled i, ii, and iii) correspond to CL–NA NPs colocalized with the late endosome/lysosome pathway, neither pathway, or the Rab11 pathway, respectively. (C,E) Plots of the percentage of internalized CL–DNA NPs that are colocalized with one of the labeled endosomal pathways or neither pathway. Black arrows highlight statistically significant increases and decreases in colocalization. (D,F) Plots of the total number of Cy5-labeled objects detected within the cell boundary. The control sample (gray) shown in all plots contained 10 mol% P2000-L (SEA-PEG). Compared to the control, a smaller number of NPs within the cells was observed for all NPs containing DEA-PEG. The first set of colocalization data (C,D) was obtained for CL–DNA NPs prepared from cationic liposomes of a molar composition of 10/80/10 MVL5/DOPC/P2000-L (control) or 11/84/5 MVL5/DOPC/DEA-PEG at a CL/DNA charge ratio of ρ=5 (same as in Figure 10). For these samples, only NPs prepared with L-P4600-L and L'-P4600-L were internalized in numbers sufficient to obtain statistically significant colocalization data. These CL–NA NPs containing 5 mol% DEA-PEG showed decreased Lysotracker colocalization as well as an increase in the fraction of particles not colocalized with either labeled pathway ("Neither"). The second set of colocalization data (E,F) was obtained for CL–DNA NPs prepared from cationic liposomes of a molar composition of 10/82/5/3 MVL5/DOPC/P2000-L/DEA-PEG at a CL/DNA charge ratio of ρ=5 (same as in Figure 10; same control as for C,D). The added SEA-PEG provides steric repulsion to temper the attractive interactions conferred by the DEA-PEGs, and these NPs were internalized to an extent sufficient for obtaining colocalization data for all four DEA-PEGs (but still less than the control). Again, incorporation of DEA-PEG significantly decreased colocalization with the late endosome/lysosome pathway and also resulted in an increased number of particles not colocalized with either labeled pathway, but only for the asymmetric DEA-PEGs, i.e., L'-P2000-L and L'-P4600-L. Rab11 colocalization did not change significantly between control and any of the DEA-PEG-containing NPs.

In previous studies, it was found that increasing membrane charge density (σ_M; tuned by NP composition) of CL–DNA NPs from low to high increased colocalization with the late endosome/lysosome pathway and transfection efficiency (the ability to transfer DNA into cells followed by expression), while increased colocalization with the Rab11 recycling pathway at low σ_M was correlated with lower transfection efficiency.[38] (The association of successful gene delivery and transfection with the late endosome/lysosome pathway has also been shown in other studies using orthogonal measurements and experimental designs.[36,68]) The underlying mechanism was hypothesized to be an increase in attractive electrostatic interactions between the CL–DNA NPs and the anionic endosomal membranes,[57] resulting in membrane fusion and endosomal escape.

Here, we sought to determine whether a similar effect could be achieved with DEA-PEGs, which increase attractive interactions due to their ability to tether two membranes in close proximity and potentially increase rates of membrane fusion. Unexpectedly, NPs containing DEA-PEGs colocalize less with the

late endosome/lysosome (Lysotracker) pathway and correspondingly more with neither labeled pathway. One interpretation of this result is that CL–DNA NPs containing DEA-PEGs formed physical cross-bridges with the endosomal membranes, tethering the two membranes in close proximity and thereby promoting membrane fusion and endosomal escape. If this happened on a sufficiently short time scale, it would decrease colocalization with Lysotracker by increasing the number of NPs in the cytoplasm, i.e., NPs not colocalized with either of the labeled endosomal pathways. Similarly, NPs fusing with the plasma membrane would directly enter the cytoplasm. Further study is required to determine whether CL–DNA NPs associated with neither endosomal pathway are indeed in the cytoplasm or are located in other organelles. Nonetheless, our study represents necessary first steps in understanding the possibilities that DEA-PEGs open for assembly of lipid-based building blocks and carriers of drugs and NAs.

In more general terms, the results of the colocalization studies prove that the addition of DEA-PEGs has a significant effect on the interactions of CL–DNA NPs with cells and the membranes within cells. NPs containing only DEA-PEG (at 5 mol%) have drastically altered interactions with the plasma and (demonstrated for L/L'-P4600-L by quantitative colocalization) endosomal membranes. Further, the experiments show that the interactions induced by the DEA-PEGs can be modulated by the structure of the DEA-PEG and the composition of the particle's corona: adding SEA-PEG addressed the problem that cell uptake was strongly reduced by too much NP aggregation. The fact that in this case only the asymmetric (L'-PEG-L) DEA-PEGs resulted in significantly different interactions with endosomal membranes again demonstrates the value of using different anchoring moieties to vary the energy barrier to entering the intermediate conformation (and thereby increase the rates of interchange between the bridging and looping conformations).

Conclusion

In this work we demonstrated that, even in dilute liposomal preparations, the addition of DEA-PEGs induces tunable attractive interactions and assembly, forming tethered structures in a variety of systems such as neutral and cationic liposomes and CL–DNA NPs). Furthermore, when incorporated into CL–DNA NPs (a lipid-based gene delivery vehicle), DEA-PEGs could modulate the NPs' interactions with cellular membranes and endosomal trafficking, as shown by colocalization analysis of CL–DNA NPs with recycling (Rab11-GFP) and late endosome/lysosomal (LysoTracker) pathways. This attraction again could be tuned by addition of repulsive steric interactions (via SEA-PEGs). The strong NP aggregation induced by DEA-PEG-directed assembly reduced cellular uptake of the NPs while also altering the intracellular fate of a fraction of the NPs. The addition of repulsive steric interactions with SEA-PEGs limited aggregation and increased uptake while maintaining the altered intracellular fate for asymmetric

DEA-PEG. Future studies will aim to identify the location of NP carriers that colocalized with neither labeled pathways probed in this work to provide a more comprehensive understanding of the influence of NP composition on pathway selection and transfection efficiency.

In our SAXS studies we investigated DEA-PEG-induced tethering in two extremes of electrostatic screening conditions. In deionized water, the CLs with DEA-PEGs are in the weak screening limit due to the presence of counterions from the cationic lipid. In this limit of weak screening (with a Debye screening length of the order of ≈1000 nm), electrostatic forces are long-range and strong. In the experiments with neutral lipids, the electrostatic forces are effectively zero (equivalent to an extremely small Debye length of the order of ≈1 Å). The SAXS data shows that tethering due to DEA-PEGs occurs in both limits even though it is much weaker for the cationic liposomes with DEA-PEG due to the presence of strong electrostatic repulsions. Based on this finding, we would expect tethering to also occur at physiological ionic strengths (of the order of 100 to 150 mM of a 1:1 salt; Debye length of the order of ≈1 nm). Indeed, the cell-based experiments confirm this, as we see evidence of tethering by DEA-PEGs in the presence of DMEM cell culture medium, which has an ionic strength of ≈150 mM.

The concept of using synthetic tethering macromolecules has the potential to open new avenues in hierarchical self-assembly in complex functional materials and separately toward enhancing the efficacy of lipid-based carriers of NAs and drugs. Importantly, DEA-PEGs are compatible with other lipid-based strategies, such as peptide-PEG-lipids with tissue-, tumor-, or cell-penetrating peptides. In fact, the incorporation of tethering DEA-PEGs into lipid-based CL–NA vectors mimics, albeit in a much simplified manner, the first stage of the retroviral approach to membrane fusion and endosomal escape. The transmembrane protein within the envelope membrane of retroviruses contains a protruding external domain consisting of a hydrophilic protein segment followed by a shorter hydrophobic segment at the N-terminus. This hydrophobic segment is designed to insert into the host plasma membrane, effectively tethering the virus to the host. The tethering is followed by the initiation of fusion of the envelope and cell plasma membranes, which involves fusogenic membrane-associated proteins.[69,70]

Our experiments have shown that the structure–property relationships of the DEA-PEGs are complex and can differ depending on the system. Further studies, likely combining empirical testing of formulations with analytical theory or computer modeling are necessary to arrive at guidelines for predicting compositions for applications in hierarchical assembly or delivery.

Supporting Information Available

Chemical structures all lipids used in this work; cryo-EM of a sonicated suspension of an MVL5/DOPC (10/90, mol/mol) lipid mixture; photographs of quartz capillaries containing suspensions of neutral liposomes for SAXS measurements; low and intermediate magnification cryo-EM micrographs of CL–DNA complexes.

Acknowledgments

This work was supported by the US Department of Energy (DOE), Office of Basic Energy Sciences, Division of Materials Sciences and Engineering, under Award DE-FG02-06ER46314 (self- and directed assembly in biomimetic charged biomolecular materials systems studied by synchrotron X-ray scattering and cryogenic TEM). The work was also supported by the National Institutes of Health under Award R01GM130769 (confocal microscopy study of CL–DNA NPs and their pathways). Partial support was further provided by the US National Science Foundation (NSF) under Award DMR-1807327 (membrane phase behavior). EW was supported in part by the National Science Foundation Graduate Research Fellowship Program under Grant No. DGE 1144085. The X-ray diffraction work was carried out at the Stanford Synchrotron Radiation Lightsource, a Directorate of SLAC National Accelerator Laboratory and an Office of Science User Facility operated for the U.S. DOE Office of Science by Stanford University. Cryo-EM experiments were conducted at the Simons Electron Microscopy Center and National Resource for Automated Molecular Microscopy located at the New York Structural Biology Center, supported by grants from the Simons Foundation (SF349247) and the NIH National Institute of General Medical Sciences (GM103310). We acknowledge the use of the NRI-MCDB Microscopy Facility at the University of California, Santa Barbara for confocal microscopy experiments.

References

1. Sercombe, L.; Veerati, T.; Moheimani, F.; Wu, S. Y.; Sood, A. K.; Hua, S.: Advances and Challenges of Liposome Assisted Drug Delivery. *Front. Pharmacol.* **2015**, *6*. DOI: 10.3389/fphar.2015.00286.
2. Allen, T. M.; Cullis, P. R.: Liposomal Drug Delivery Systems: From Concept to Clinical Applications. *Adv. Drug Delivery Rev.* **2013**, *65*, 36-48. DOI: 10.1016/j.addr.2012.09.037.
3. Wan, C.; Allen, T. M.; Cullis, P. R.: Lipid nanoparticle Delivery Systems for siRNA-based Therapeutics. *Drug Delivery Transl. Res.* **2014**, *4*, 74-83. DOI: 10.1007/s13346-013-0161-z.
4. Safinya, C. R.; Ewert, K. K.; Majzoub, R. N.; Leal, C.: Cationic Liposome-Nucleic Acid Complexes for Gene Delivery and Gene Silencing. *New J. Chem.* **2014**, *38*, 5164-5172. DOI: 10.1039/c4nj01314j.

5. Geinguenaud, F.; Guenin, E.; Lalatonne, Y.; Motte, L.: Vectorization of Nucleic Acids for Therapeutic Approach: Tutorial Review. *ACS Chem. Biol.* **2016**, *11*, 1180-1191. DOI: 10.1021/acschembio.5b01053.
6. Yin, H.; Kauffman, K. J.; Anderson, D. G.: Delivery Technologies for Genome Editing. *Nat. Rev. Drug Discovery* **2017**, *16*, 387-399. DOI: 10.1038/nrd.2016.280.
7. Guan, S.; Rosenecker, J.: Nanotechnologies in Delivery of mRNA Therapeutics Using Nonviral Vector-Based Delivery Systems. *Gene Ther.* **2017**, *24*, 133-143. DOI: 10.1038/gt.2017.5.
8. Yin, H.; Kanasty, R. L.; Eltoukhy, A. A.; Vegas, A. J.; Dorkin, J. R.; Anderson, D. G.: Non-Viral Vectors for Gene-Based Therapy. *Nat. Rev. Genet.* **2014**, *15*, 541-555. DOI: 10.1038/nrg3763.
9. Wang, Y.; Miao, L.; Satterlee, A.; Huang, L.: Delivery of Oligonucleotides with Lipid Nanoparticles. *Adv. Drug Delivery Rev.* **2015**, *87*, 68-80. DOI: 10.1016/j.addr.2015.02.007.
10. Guo, X.; Huang, L.: Recent Advances in Nonviral Vectors for Gene Delivery. *Acc. Chem. Res.* **2012**, *45*, 971-979. DOI: 10.1021/ar200151m.
11. Bielke, W.; Erbacher, C., Eds.: *Nucleic Acid Transfection*. Springer: Berlin, **2010**.
12. Draghici, B.; Ilies, M. A.: Synthetic Nucleic Acid Delivery Systems: Present and Perspectives. *J. Med. Chem.* **2015**. DOI: 10.1021/jm500330k.
13. Harrington, J. J.; Van Bokkelen, G.; Mays, R. W.; Gustashaw, K.; Willard, H. F.: Formation of De Novo Centromeres and Construction of First-Generation Human Artificial Microchromosomes. *Nat. Genet.* **1997**, *15*, 345-355. DOI: 10.1038/ng0497-345.
14. Thomas, C. E.; Ehrhardt, A.; Kay, M. A.: Progress and Problems with the Use of Viral Vectors for Gene Therapy. *Nat. Rev. Genet.* **2003**, *4*, 346-358. DOI: 10.1038/nrg1066.
15. Hacein-Bey-Abina, S.; Garrigue, A.; Wang, G. P.; Soulier, J.; Lim, A.; Morillon, E.; Clappier, E.; Caccavelli, L.; Delabesse, E.; Beldjord, K.; Asnafi, V.; Macintyre, E.; Dal Cortivo, L.; Radford, I.; Brousse, N.; Sigaux, F.; Moshous, D.; Hauer, J.; Borkhardt, A.; Belohradsky, B. H.; Wintergerst, U.; Velez, M. C.; Leiva, L.; Sorensen, R.; Wulffraat, N.; Blanche, S.; Bushman, F. D.; Fischer, A.; Cavazzana-Calvo, M.: Insertional Oncogenesis in 4 Patients after Retrovirus-Mediated Gene Therapy of SCID-X1. *J. Clin. Invest.* **2008**, *118*, 3132-3142. DOI: 10.1172/jc135700.
16. Li, S.-D.; Huang, L.: Non-viral is Superior to Viral Gene Delivery. *J. Controlled Release* **2007**, *123*, 181-183. DOI: 10.1016/j.jconrel.2007.09.004.
17. Hoy, S. M.: Patisiran: First Global Approval. *Drugs* **2018**, *78*, 1625-1631. DOI: 10.1007/s40265-018-0983-6.
18. Edelstein, M. L.; Abedi, M. R.; Wixon, J.; Edelstein, R. M.: Gene Therapy Clinical Trials Worldwide 1989–2004—an Overview. *J. Gene Med.* **2004**, *6*, 597-602. DOI: 10.1002/jgm.619.
19. Ginn, S. L.; Amaya, A. K.; Alexander, I. E.; Edelstein, M.; Abedi, M. R.: Gene Therapy Clinical Trials Worldwide to 2017: An Update. *J. Gene Med.* **2018**, *20*, e3015. DOI: 10.1002/jgm.3015.
20. Klibanov, A. L.; Maruyama, K.; Torchilin, V. P.; Huang, L.: Amphipathic Polyethyleneglycols Effectively Prolong the Circulation Time of Liposomes. *FEBS Lett.* **1990**, *268*, 235-237. DOI: 10.1016/0014-5793(90)81016-h.
21. Blume, G.; Cevc, G.: Liposomes for the Sustained Drug Release In Vivo. *Biochim. Biophys. Acta, Biomembr.* **1990**, *1029*, 91-97. DOI: 10.1016/0005-2736(90)90440-Y.
22. Papahadjopoulos, D.; Allen, T. M.; Gabizon, A.; Mayhew, E.; Matthay, K.; Huang, S. K.; Lee, K. D.; Woodle, M. C.; Lasic, D. D.; Redemann, C.: Sterically Stabilized Liposomes: Improvements in

Pharmacokinetics and Antitumor Therapeutic Efficacy. *Proc. Natl. Acad. Sci. U. S. A.* **1991**, *88*, 11460-11464.

23. Allen, T. M.; Hansen, C.; Martin, F.; Redemann, C.; Yau-Young, A.: Liposomes Containing Synthetic Lipid Derivatives of Poly(Ethylene Glycol) Show Prolonged Circulation Half-Lives In Vivo. *Biochim. Biophys. Acta, Biomembr.* **1991**, *1066*, 29-36. DOI: 10.1016/0005-2736(91)90246-5.
24. Woodle, M. C.; Lasic, D. D.: Sterically Stabilized Liposomes. *Biochim. Biophys. Acta* **1992**, *1113*, 171-199. DOI: 10.1016/0304-4157(92)90038-c.
25. Lasic, D. D.; Needham, D.: The "Stealth" Liposome: A Prototypical Biomaterial. *Chem. Rev.* **1995**, *95*, 2601-2628. DOI: 10.1021/cr00040a001.
26. Silvander, M.: Steric Stabilization of Liposomes — a Review. *Prog. Colloid Polym. Sci.* **2002**, *120*, 35-40. DOI: 10.1007/3-540-45291-5_5.
27. Needham, D.; McIntosh, T. J.; Lasic, D. D.: Repulsive Interactions and Mechanical Stability of Polymer-Grafted Lipid Membranes. *Biochim. Biophys. Acta, Biomembr.* **1992**, *1108*, 40-48. DOI: 10.1016/0005-2736(92)90112-Y.
28. Kuhl, T. L.; Leckband, D. E.; Lasic, D. D.; Israelachvili, J. N.: Modulation of Interaction Forces between Bilayers Exposing Short-Chained Ethylene Oxide headgroups. *Biophys. J.* **1994**, *66*, 1479-1488. DOI: 10.1016/S0006-3495(94)80938-5.
29. Zhang, L.; Gu, F. X.; Chan, J. M.; Wang, A. Z.; Langer, R. S.; Farokhzad, O. C.: Nanoparticles in Medicine: Therapeutic Applications and Developments. *Clin. Pharmacol. Ther.* **2007**, *83*, 761-769.
30. Silva, B. F. B.; Majzoub, R. N.; Chan, C.-L.; Li, Y.; Olsson, U.; Safinya, C. R.: PEGylated Cationic Liposome–DNA Complexation in Brine is Pathway-Dependent. *Biochim. Biophys. Acta, Biomembr.* **2014**, *1838*, 398-412. DOI: 10.1016/j.bbamem.2013.09.008.
31. Majzoub, R. N.; Ewert, K. K.; Jacovetty, E. L.; Carragher, B.; Potter, C. S.; Li, Y.; Safinya, C. R.: Patterned Threadlike Micelles and DNA-Tethered Nanoparticles: A Structural Study of PEGylated Cationic Liposome–DNA Assemblies. *Langmuir* **2015**, *31*, 7073-7083. DOI: 10.1021/acs.langmuir.5b00993.
32. Martin-Herranz, A.; Ahmad, A.; Evans, H. M.; Ewert, K.; Schulze, U.; Safinya, C. R.: Surface Functionalized Cationic Lipid-DNA Complexes for Gene Delivery: PEGylated Lamellar Complexes Exhibit Distinct DNA-DNA Interaction Regimes. *Biophys. J.* **2004**, *86*, 1160-1168. DOI: 10.1016/S0006-3495(04)74190-9.
33. Chan, C.-L.; Majzoub, R. N.; Shirazi, R. S.; Ewert, K. K.; Chen, Y.-J.; Liang, K. S.; Safinya, C. R.: Endosomal Escape and Transfection Efficiency of PEGylated Cationic Liposome–DNA Complexes Prepared with an Acid-Labile PEG-Lipid. *Biomaterials* **2012**, *33*, 4928-4935. DOI: 10.1016/j.biomaterials.2012.03.038.
34. Majzoub, R. N.; Chan, C.-L.; Ewert, K. K.; Silva, B. F. B.; Liang, K. S.; Jacovetty, E. L.; Carragher, B.; Potter, C. S.; Safinya, C. R.: Uptake and Transfection Efficiency of PEGylated Cationic Liposome–DNA Complexes with and without RGD-Tagging. *Biomaterials* **2014**, *35*, 4996-5005. DOI: 10.1016/j.biomaterials.2014.03.007.
35. Shete, H. K.; Prabhu, R. H.; Patravale, V. B.: Endosomal Escape: A Bottleneck in Intracellular Delivery. *J. Nanosci. Nanotechnol.* **2014**, *14*, 460-474. DOI: 10.1166/jnn.2014.9082.
36. Wittrup, A.; Ai, A.; Liu, X.; Hamar, P.; Trifonova, R.; Charisse, K.; Manoharan, M.; Kirchhausen, T.; Lieberman, J.: Visualizing Lipid-Formulated siRNA Release from Endosomes and Target Gene Knockdown. *Nat. Biotech.* **2015**, *33*, 870-876. DOI: 10.1038/nbt.3298.

37. Ewert, K. K.; Kotamraju, V. R.; Majzoub, R. N.; Steffes, V. M.; Wonder, E. A.; Teesalu, T.; Ruoslahti, E.; Safinya, C. R.: Synthesis of Linear and Cyclic Peptide–PEG–Lipids for Stabilization and Targeting of Cationic Liposome–DNA Complexes. *Bioorg. Med. Chem. Lett.* **2016**, *26*, 1618-1623. DOI: 10.1016/j.bmcl.2016.01.079.
38. Majzoub, R. N.; Wonder, E.; Ewert, K. K.; Kotamraju, V. R.; Teesalu, T.; Safinya, C. R.: Rab11 and Lysotracker Markers Reveal Correlation between Endosomal Pathways and Transfection Efficiency of Surface-Functionalized Cationic Liposome–DNA Nanoparticles. *J. Phys. Chem. B* **2016**, *120*, 6439-6453. DOI: 10.1021/acs.jpcb.6b04441.
39. Wonder, E.; Simón-Gracia, L.; Scodeller, P.; Majzoub, R. N.; Kotamraju, V. R.; Ewert, K. K.; Teesalu, T.; Safinya, C. R.: Competition of Charge-Mediated and Specific Binding by Peptide-Tagged Cationic Liposome–DNA Nanoparticles In Vitro and In Vivo. *Biomaterials* **2018**, *166*, 52-63. DOI: 10.1016/j.biomaterials.2018.02.052.
40. Sugahara, K. N.; Teesalu, T.; Karmali, P. P.; Kotamraju, V. R.; Agemy, L.; Girard, O. M.; Hanahan, D.; Mattrey, R. F.; Ruoslahti, E.: Tissue-Penetrating Delivery of Compounds and Nanoparticles into Tumors. *Cancer Cell* **2009**, *16*, 510-520. DOI: 10.1016/j.ccr.2009.10.013.
41. Ruoslahti, E.; Bhatia, S. N.; Sailor, M. J.: Targeting of Drugs and Nanoparticles to Tumors. *J. Cell Biol.* **2010**, *188*, 759-768. DOI: 10.1083/jcb.200910104.
42. Peer, D.; Karp, J. M.; Hong, S.; Farokhzad, O. C.; Margalit, R.; Langer, R.: Nanocarriers as an Emerging Platform for Cancer Therapy. *Nat. Nanotechnol.* **2007**, *2*, 751-760.
43. Glass, J. E.: A Perspective on the History of and Current Research in Surfactant-Modified, Water-soluble Polymers. *J. Coat. Technol.* **2001**, *73*, 79-98. DOI: 10.1007/bf02698434.
44. Winnik, M. A.; Yekta, A.: Associative Polymers in Aqueous Solution. *Curr. Opin. Colloid Interface Sci.* **1997**, *2*, 424-436. DOI: https://doi.org/10.1016/S1359-0294(97)80088-X.
45. Rubinstein, M.; Dobrynin, A. V.: Solutions of Associative Polymers. *Trends Polym. Sci. (Cambridge, U. K.)* **1997**, *5*, 181-186.
46. Séréro, Y.; Aznar, R.; Porte, G.; Berret, J. F.; Calvet, D.; Collet, A.; Viguier, M.: Associating Polymers: From "Flowers" to Transient Networks. *Phys. Rev. Lett.* **1998**, *81*, 5584-5587. DOI: 10.1103/PhysRevLett.81.5584.
47. Auguste, D. T.; Prud'homme, R. K.; Ahl, P. L.; Meers, P.; Kohn, J.: Polymer-Protected Liposomes: Association of Hydrophobically-Modified PEG with Liposomes. In *Polymeric Drug Delivery I*, American Chemical Society: **2006**; pp. 95-120. DOI: doi:10.1021/bk-2006-0923.ch008.
48. Slack, N. L.; Davidson, P.; Chibbaro, M. A.; Jeppesen, C.; Eiselt, P.; Warriner, H. E.; Schmidt, H. W.; Pincus, P.; Safinya, C. R.: The Bridging Conformations of Double-End Anchored Polymer-Surfactants Destabilize a Hydrogel of Lipid Membranes. *J. Chem. Phys.* **2001**, *115*, 6252-6257. DOI: 10.1063/1.1399061.
49. Slack, N. L.; Schellhorn, M.; Eiselt, P.; Chibbaro, M. A.; Schulze, U.; Warriner, H. E.; Davidson, P.; Schmidt, H. W.; Safinya, C. R.: Synthesis and Phase Behavior of New Amphiphilic PEG-Based Triblock Copolymers as Gelling Agents for Lamellar Liquid Crystalline Phases. *Macromolecules* **1998**, *31*, 8503-8508. DOI: 10.1021/ma980901g.
50. Liu, C.; Ewert, K. K.; Wonder, E.; Kohl, P.; Li, Y.; Qiao, W.; Safinya, C. R.: Reversible Control of Spacing in Charged Lamellar Membrane Hydrogels by Hydrophobically Mediated Tethering with Symmetric and Asymmetric Double-End-Anchored Poly(ethylene glycol)s. *ACS Appl. Mater. Interfaces* **2018**, *10*, 44152-44162. DOI: 10.1021/acsami.8b16456.

51. Majzoub, R. N.; Ewert, K. K.; Safinya, C. R.: Quantitative Intracellular Localization of Cationic Lipid-Nucleic Acid Nanoparticles with Fluorescence Microscopy. In *Non-Viral Gene Delivery Vectors: Methods and Protocols*, Candiani, G., Ed. Springer/Humana Press: New York, **2016**; pp. 77-108. DOI: 10.1007/978-1-4939-3718-9_6.
52. Ewert, K.; Ahmad, A.; Evans, H. M.; Schmidt, H. W.; Safinya, C. R.: Efficient Synthesis and Cell-Transfection Properties of a New Multivalent Cationic Lipid for nonviral gene delivery. *J. Med. Chem.* **2002**, *45*, 5023-5029. DOI: 10.1021/jm020233w.
53. Ilavsky, J.: Nika: Software for Two-Dimensional Data Reduction. *J. Appl. Crystallogr.* **2012**, *45*, 324-328. DOI: 10.1107/S0021889812004037.
54. Ilavsky, J.; Jemian, P. R.: Irena: Tool Suite for Modeling and Analysis of Small-Angle Scattering. *J. Appl. Crystallogr.* **2009**, *42*, 347-353. DOI: 10.1107/S0021889809002222.
55. Fukami, A.; Adachi, K.: A New Method of Preparation of a Self-Perforated Micro Plastic Grid and its Application. *J. Electron Microsc.* **1965**, *14*, 112-118. DOI: 10.1093/oxfordjournals.jmicro.a049472.
56. Suloway, C.; Pulokas, J.; Fellmann, D.; Cheng, A.; Guerra, F.; Quispe, J.; Stagg, S.; Potter, C. S.; Carragher, B.: Automated Molecular Microscopy: The New Leginon System. *J. Struct. Biol.* **2005**, *151*, 41-60.
57. Majzoub, R. N.; Chan, C.-L.; Ewert, K. K.; Silva, B. F. B.; Liang, K. S.; Safinya, C. R.: Fluorescence Microscopy Colocalization of Lipid–Nucleic Acid Nanoparticles with Wildtype and Mutant Rab5–GFP: A Platform for Investigating Early Endosomal Events. *Biochim. Biophys. Acta, Biomembr.* **2015**, *1848*, 1308-1318. DOI: 10.1016/j.bbamem.2015.03.001.
58. Majzoub, R. N. Investigating Intracellular Pathways of Surface-Functionalized Cationic Lipid-DNA Nanoparticles using Quantitative Fluorescence Microscopy. University of California at Santa Barbara, Santa Barbara, 2015.
59. Crocker, J. C.; Grier, D. G.: Methods of Digital Video Microscopy for Colloidal Studies. *J. Colloid Interface Sci.* **1996**, *179*, 298-310. DOI: 10.1006/jcis.1996.0217.
60. Steffes, V. M.; Zhang, Z.; MacDonald, S.; Crowe, J.; Ewert, K. K.; Carragher, B.; Potter, C. S.; Safinya, C. R.: PEGylation of Paclitaxel-Loaded Cationic Liposomes Drives Steric Stabilization of Bicelles and Vesicles thereby Enhancing Delivery and Cytotoxicity to Human Cancer Cells. *ACS Appl. Mater. Interfaces* **2020**, *12*, 151-162. DOI: 10.1021/acsami.9b16150.
61. Ahmad, A.; Evans, H. M.; Ewert, K.; George, C. X.; Samuel, C. E.; Safinya, C. R.: New Multivalent Cationic Lipids Reveal Bell Curve for Transfection Efficiency versus Membrane Charge Density: Lipid - DNA complexes for gene delivery. *J. Gene. Med.* **2005**, *7*, 739-748. DOI: 10.1002/jgm.717.
62. Chaikin, P. M.; Lubensky, T. C.: *Principles of Condensed Matter Physics*. Cambridge University Press: Cambridge, **1995**. DOI: 10.1017/CBO9780511813467.
63. Rädler, J. O.; Koltover, I.; Salditt, T.; Safinya, C. R.: Structure of DNA-Cationic Liposome Complexes: DNA Intercalation in Multilamellar Membranes in Distinct Interhelical Packing Regimes. *Science* **1997**, *275*, 810-814. DOI: 10.1126/science.275.5301.810.
64. Doherty, G. J.; McMahon, H. T.: Mechanisms of Endocytosis. *Annu. Rev. Biochem.* **2009**, *78*, 857-902. DOI: 10.1146/annurev.biochem.78.081307.110540.
65. Stenmark, H.; Olkkonen, V. M.: The Rab GTPase Family. *Genome Biol.* **2001**, *2*, reviews3007--reviews3007.7. DOI: 10.1186/gb-2001-2-5-reviews3007.
66. Stenmark, H.: Rab GTPases as Coordinators of Vesicle Traffic. *Nat. Rev. Mol. Cell Biol.* **2009**, *10*, 513-525. DOI: 10.1038/nrm2728.

67. Wandinger-Ness, A.; Zerial, M.: Rab Proteins and the Compartmentalization of the Endosomal System. *Cold Spring Harbor Perspect. Biol.* **2014**, *6*. DOI: 10.1101/cshperspect.a022616.

68. Patel, S.; Ashwanikumar, N.; Robinson, E.; DuRoss, A.; Sun, C.; Murphy-Benenato, K. E.; Mihai, C.; Almarsson, Ö.; Sahay, G.: Boosting Intracellular Delivery of Lipid Nanoparticle-Encapsulated mRNA. *Nano Lett.* **2017**, *17*, 5711-5718. DOI: 10.1021/acs.nanolett.7b02664.

69. Fields, B. N.; Knipe, D. M.; Howley, P. M., Eds.: *Fundamental Virology*. 3rd ed.; Lippincott Williams & Wilkins: New York, **1996**.

70. Freed, E. O.; Myers, D. J.; Risser, R.: Characterization of the Fusion Domain of the Human Immunodeficiency Virus Type 1 Envelope Glycoprotein gp41. *Proc. Natl. Acad. Sci. U. S. A.* **1990**, *87*, 4650-4654. DOI: 10.1073/pnas.87.12.4650.

For Table of Contents Only